View Article Online / Journal Homepage / Table of Contents for this issue
Dynamic Article Links

PCCP

Cite this: *Phys. Chem. Chem. Phys.*, 2012, **14**, 1985–2000

www.rsc.org/pccp

PAPER

Bonding situation and N–O-bond strengths in amine-*N*-oxides—a combined experimental and theoretical study†

Andrey Yu. Rogachev and Peter Burger*

Received 19th July 2011, Accepted 6th December 2011
DOI: 10.1039/c2cp22341d

Published on 10 January 2012 on http://pubs.rsc.org | doi:10.1039/C2CP22341D
Downloaded by Universite de Picardie on 27 November 2012

The bonding situation and energetics of the N–O bond in a series of amine-*N*-oxides, $Ph_x(CH_3)_{3-x}N$–O, where x = 0–3, were analyzed experimentally and theoretically. There is a notable nearly linear decrease of the N–O bond dissociation energies (BDEs) for this series with an increasing number of phenyl groups x. This was investigated experimentally by X-ray high angle multipole refinement techniques in combination with subsequent topological analysis of the electron density for the representative $(CH_3)_2PhN$–O, **2**, and complementary theoretical calculations at the DFT and multireference CASSCF and MR-perturbation theory (MCQDPT2) levels. Both the theoretical and experimental results unambiguously revealed a polar covalent σ-bond for the N–O bond with an essentially identical bonding situation for all amine-*N*-oxides studied. This apparent disparity between the bonding situation and the trend of BDEs is attributed to the large differences of the relaxation energies of the corresponding amines $Ph_x(CH_3)_{3-x}N$, (x = 0–3), respectively, the required preparation energies (ΔE_{prep}) for the reverse N–O bond forming process. The detailed theoretical analysis of the amines allowed us to trace the trend of larger values of ΔE_{prep} for a higher number of phenyl groups x to an increase of $n(N) \rightarrow \pi^*(C–C)$ delocalization interactions.

Introduction

Amine-*N*-oxides represent an interesting class of compounds and are widely applied in biological applications and in catalysis as well as synthetic tools. For instance, trimethylamine-*N*-oxide, $(CH_3)_3N$–O, is also discussed as prodrug in cancer therapy[1] and was found to stabilize proteins[2] as well as to counteract the influence of urea in biological systems.[3] Moreover, even refolding of denaturized proteins has been ascribed to this compound.[4] The study of the biological activity of this amine-*N*-oxide molecule is ongoing with some interesting details recently being elucidated through molecular dynamic simulations.[4,5] Apparently, the stabilization of proteins by $(CH_3)_3N$–O is not due to direct interaction with proteins itself but is rather based on strong hydrogen bonding to water. This leads to changes in the aggregation properties of the latter, which in turn has a strong influence on the stability of the protein.

In the field of inorganic and organometallic chemistry, previous studies showed that $(CH_3)_3N$–O is a strong nucleophile and also acts as a good oxidizing reagent through oxygen atom transfer. The decarbonylation reaction in organometallic chemistry,[6] $M(CO)_n + (CH_3)_3N–O \rightarrow M(CO)_{n-1}(N(CH_3)_3) + CO_2$, which proceeds by release of the carbonyl ligand as CO_2 and concomitant reduction of $(CH_3)_3N$–O to $(CH_3)_3N$ is an excellent example for this type of reactivity. This unusual property of trimethylamine-*N*-oxide, *i.e.* being both a good nucleophile and a good oxidizing reagent raises the question on the nature of its N–O bond. Nevertheless, in spite of the wide use of trimethylamine-*N*-oxide and its alkyl substituted derivatives in different fields of chemistry and biology, just a few studies were devoted to theoretical investigations of the nature and energetics of the N–O bond in these systems,[7] in contrast to the comprehensively studied pyridine-*N*-oxide, its derivatives and other heterocyclic analogues.[8]

This prompted us to perform an *in-depth* experimental and theoretical analysis of the inherent electronic structure of the N–O bonds in alkyl amine-*N*-oxide systems, which were considered as benchmark for a covalent bond with a strong $R_3N^{\delta+}–O^{\delta-}$ polarization. In particular, we were interested in the influence of the substituents on the N–O bond dissociation enthalpy (BDE). For this study, the series of amine-*N*-oxides shown in Scheme 1 were chosen, in which the methyl groups were successively replaced by phenyl substituents. Herein, we present X-ray crystal structures for two new phenyl substituted members of the series.

This study was extended to a precision high-angle X-ray experiment with subsequent multipole refinement and complemented by a full topological analysis of the experimental

Institut für Anorganische und Angewandte Chemie, Universität Hamburg, 20146 Hamburg, Germany. E-mail: burger@chemie.uni-hamburg.de

† Electronic supplementary information (ESI) available. See DOI: 10.1039/c2cp22341d

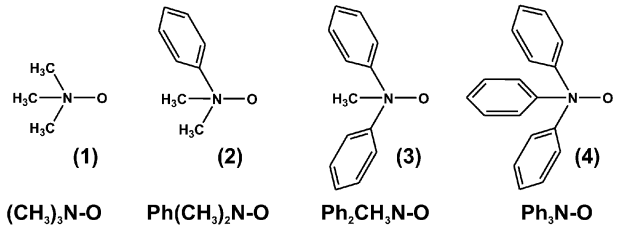

Scheme 1

electron density in terms of Bader's Quantum Theory of Atoms In Molecules (QTAIM).[9] In support of the experimental study, a comprehensive theoretical analysis of the nature and the energetics of the N–O bond in this type of *N*-oxides was carried out by a number of theoretical approaches, *i.e.* from standard (single-reference) density functional theory (DFT) methods to highly correlated multi-reference (MR) techniques, *e.g.* CASSCF and MR second-order perturbation theory.

Results and discussion

As the first step of this study, the dependence of the N–O bond dissociation enthalpy (BDE) on the number of phenyl groups x of the series of amine-*N*-oxide derivatives **1–4** was investigated by means of different hybrid functionals as well as the Hartree–Fock method. The energetics are based on the dissociation process of the amine-*N*-oxides **1–4** to the corresponding amines and dioxygen according to eqn (1).

$$Ph_x(CH_3)_{3-x}N\text{–}O \rightarrow Ph_x(CH_3)_{3-x}N + \tfrac{1}{2}\,{}^3O_2 \qquad (1)$$

Independent of the applied theoretical methodology, these calculations revealed a previously unknown approximately linear correlation between the number of phenyl groups x and the N–O bond strength (Fig. 1).

We have deliberately selected dioxygen ($^3O_2$) and not the oxygen atom in its ^3P ground state as the product in eqn (1), in order to highlight the fact that the known amine-*N*-oxides **1–3** are *inert* rather than *stable* molecules. This becomes readily apparent from inspection of the calculated reaction energies for the reaction according to eqn (1), which is negative for all amine-*N*-oxides of the series (Fig. 1). Since dioxygen is the common product of all amine-*N*-oxides, the *trend* of the N–O bond dissociation enthalpies in **1–4** is nevertheless correctly reproduced.

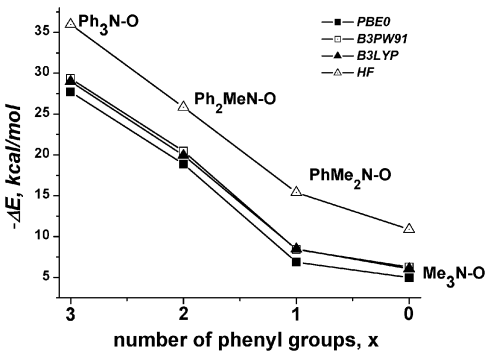

Fig. 1 Trend of the N–O bond strengths in the series of amine-*N*-oxides, $Ph_x(CH_3)_{3-x}N$–O, on the number of phenyl groups x (based on eqn (1)).

Significant weakening of the N–O bond is observed in this series upon substitution of methyl for phenyl groups. This is best exemplified by the difference of *ca.* 30 kcal mol^{-1} for the bonding energies in trimethylamine-*N*-oxide, **1**, and the triphenyl analogue **4**, which might explain that triphenylamine-*N*-oxide, **4**, is still an unknown compound to the best of our knowledge.

It deserves a special mention that Basolo *et al.* studied the decarbonylation kinetics of metal carbonyl complexes induced by the amine-*N*-oxides **1–3**.[10] Their results showed a trend, which might have anticipated based on Fig. 1: amine-*N*-oxides with weaker BDEs of the N–O bond display a higher aptitude for decarbonylation, and the order of the second-order kinetic rates is **3** > **2** > **1**.

Thus, based on these computational and experimental data, significant changes in the nature of the N–O bond in the series *might* perhaps be anticipated. Regarding this view, a word of caution seems in place, however. Since we are considering the trend of a bond breaking process, structural and electronic changes in going from the amine-*N*-oxide to the corresponding amine might rather dominate and little if any difference in the electronic structure might be prevalent in the ground states of the amine-*N*-oxides. It is therefore clear that both sides of the reaction equation have to be evaluated. In order to address this subtle point, we have firstly investigated the amine-*N*-oxides experimentally and through comprehensive quantum chemical calculations. In a second step, we turned to theoretical studies of the corresponding amines.

Within this study, the parameter free hybrid functional PBE0 was employed for geometry optimizations (Fig. 2) and for the study of the molecular orbital picture of the N–O bonding situation. Initially, the employed theoretical approach was validated by comparison of the experimental X-ray diffraction and quantum-chemically derived geometrical parameters. Further support for the validity of the theoretical approach was provided through comparison of the experimental and theoretical topological parameters of the electronic density in the amine-*N*-oxide, **2**, ($Ph(CH_3)_2N$–O, *vide infra*).

Crystal structures of 2 and 3 and validation of theory

Selected experimental geometrical parameters observed in the X-ray crystal structures of **2** and **3** along with values derived by DFT calculations for the optimized geometries in the gas phase are compiled in Table 1. The experimentally observed intramolecular C–H···O-hydrogen bonds are highlighted in Fig. 3 and will be discussed below.

The crystal structure of **2** consists of practically isolated molecules of $Ph(CH_3)_2N$–O (Fig. 3, entry (*a*)). Relatively short intermolecular O–H contacts were found between the oxygen and hydrogen atoms of the phenyl ring (2.195(13) Å) and hydrogen atoms of the methyl groups (2.465(14) Å, 2.476(13) Å and 2.521(13) Å) of neighboring molecules (see ESI† for details). Interestingly, the observed intramolecular C–H···O hydrogen bond length between the amine-*N*-oxide oxygen atom and an ortho hydrogen atom of the adjacent phenyl ring lies between the two corresponding intermolecular distances and amounts to 2.320(1) Å (d(H(4)···O(1)) 2.320(1) Å, *cf.* Fig. 3). The formed five-membered ring is almost planar displaying a

Published on 10 January 2012 on http://pubs.rsc.org | doi:10.1039/C2CP22341D
Downloaded by Universite de Picardie on 27 November 2012

 This journal is © the Owner Societies 2012

Published on 10 January 2012 on http://pubs.rsc.org | doi:10.1039/C2CP22341D
Downloaded by Universite de Picardie on 27 November 2012

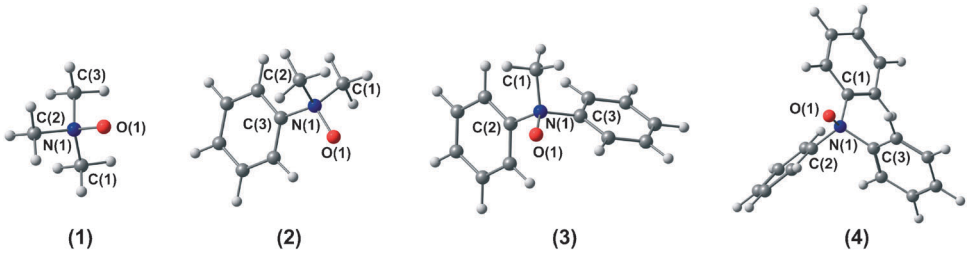

Fig. 2 Equilibrium geometries for the amine-*N*-oxides $Ph_x(CH_3)_{3-x}N$–O (**1–4**) along with the labeling scheme (DFT/PBE0).

Table 1 Selected experimental and theoretical geometrical parameters for $Ph_x(CH_3)_{3-x}N$–O (**1–4**); distances are given in [Å], angles in [°] with esd's in parentheses for the experimental values

	Compound			
Parameter	$(CH_3)_3N$–O (**1**)	$Ph(CH_3)_2N$–O (**2**)	Ph_2CH_3N–O (**3**)	Ph_3N–O (**4**)
N(1)–O(1) (theor.)	1.348	1.344	1.347	1.351
N(1)–O(1) (exp.)	1.388(5)[a]	1.388(1)	1.387(3)	
	1.379(3)[b]			
N(1)–C(1) (theor.)	1.487	1.492	1.493	1.504
N(1)–C(1) (exp.)	1.484(4)[a]	1.503(1)	1.496(4)	
	1.496(2)[b]			
N(1)–C(2) (theor.)	1.487	1.492	1.493	1.504
N(1)–C(2) (exp.)	1.484(4)[a]	1.503(1)	1.501(4)	
	1.496(2)[b]			
N(1)–C(3) (theor.)	1.487	1.498	1.507	1.504
N(1)–C(3) (exp.)	1.470(8)[a]	1.503(1)	1.508(4)	
	1.496(2)[b]			
Out-of-plane (N(1)) (theor.)	0.502	0.508	0.503	0.496
Out-of-plane (N(1)) (exp.)	0.502[b]	0.503	0.494	
POAV[11] (N) (theor.)	109.79	109.88	109.64	109.24
POAV[11] (N) (exp.)	109.86[b]	109.54	109.08	
Pyramidality index (theor.)	0.779	0.781	0.774	0.763
pyramidality index (exp.)	0.781[b]	0.771	0.760	
ν(N–O)/cm^{-1} (theor.)[c]	984	1015	1065	1010
IR: ν(N–O)/cm^{-1} (exp.)	950[d]	1020	1070	

[a] Structural parameters corresponding to the X-ray crystal structure data of $(CH_3)_3N$–O.[12] [b] Structural parameters corresponding to the gas phase electron diffraction data (GED).[7c] [c] The calculated ν(N–O) IR vibrational frequencies are unscaled. [d] The ν(N–O) IR vibrational frequency for **1** was taken from the literature.[13]

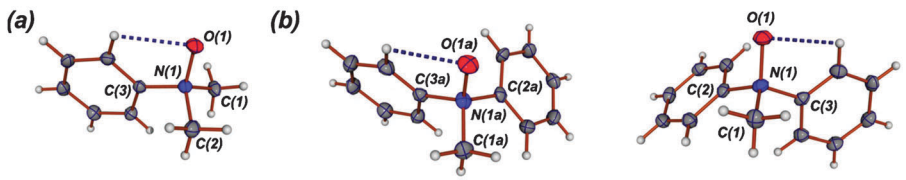

Fig. 3 X-Ray molecular structures of (a) $Ph(CH_3)_2N$–O (**2**) and (b) two optical isomers of $Ph_2(CH_3)N$–O ($\mathbf{3_I}$ and $\mathbf{3_{II}}$). Dashed lines indicate intramolecular hydrogen bonds.

dihedral angle ∠O(1)–N(1)–C(3)–C(4) 17.44(12)° with a maximal out-of-plane deviation (Δ_{max}(out-of-plane)) equal to 0.1149 Å corresponding to the nitrogen atom N(1).

The crystal structure of compound **3** contains two independent molecules of $Ph_2(CH_3)N$–O (Fig. 3, entry (*b*)). Close inspection of the latter showed that these molecules are optical isomers originating from two inequivalent phenyl substituents. This is due to an intramolecular C–H···O hydrogen bond between the oxygen atom and a hydrogen atom of one of the phenyl rings. The observed values of d(H···O) = 2.314(3) Å and 2.314(2) Å for $\mathbf{3_I}$ and $\mathbf{3_{II}}$, respectively, are slightly shorter than the related distances observed in the crystal structure of **2**. The corresponding five-membered ring encompassing the C–H···O hydrogen bond is also nearly planar (Δ_{max}(out-of-plane) = 0.0908 Å and 0.0944 Å, for $\mathbf{3_I}$ and $\mathbf{3_{II}}$, respectively) and the dihedral angles ∠O(1)–N(1)–C(3)–C(8) and ∠O(1a)–N(1a)–C(3a)–C(8a) amount to 13.3(4)° and 13.7(4)°. The values for the corresponding dihedral angles of the second phenyl substituent on the other hand are 55.6(4)° and 54.8(3)°, thus, disabling intramolecular C–H···O hydrogen bonds to the second ring. The closest intermolecular contacts between neighboring molecules were observed between the oxygen atom and (i) phenyl hydrogen atoms (2.673(3) Å and 2.669(3) Å for $\mathbf{3_I}$ and $\mathbf{3_{II}}$, respectively), and (ii) hydrogen atoms from methyl groups (2.454(3) Å, 2.321(3) Å and 2.668(2) Å for $\mathbf{3_I}$; 2.479(3) Å and 2.377(3) Å for $\mathbf{3_{II}}$).

Published on 10 January 2012 on http://pubs.rsc.org | doi:10.1039/C2CP22341D
Downloaded by Universite de Picardie on 27 November 2012

Importantly, the X-ray determined N–O bond lengths of 1.388 Å in compounds **1–3** are identical within experimental error (Table 1). Considering the trends of significantly decreasing N–O bond dissociation enthalpies in going from **1** → **3** this is at first glance remarkable and perhaps unanticipated (*cf*. Fig. 1). The DFT calculations are well consistent with this finding and display a narrow range of 1.344–1.351 Å for the N–O bond distances in compounds **1–4** (Table 1). There is, however, a notable systematic deviation of 0.04 Å between the experimental and computed values in the gas phase. It is noteworthy that the MP2-optimized geometries of the amine *N*-oxides **1–4** also revealed N–O bond distances, which are *ca*. systematically 0.02 Å shorter than the experimentally determined bond lengths. Deviations might be due to the influence of crystal packing forces or intermolecular hydrogen bonding that are not taken into account in the theoretical (gas phase) calculations. This view is supported by an exemplary periodic boundary DFT calculation (PBE0 functional) for crystalline trimethyl amine *N*-oxide **1** based on the published X-ray crystal structure, from which a longer optimized N–O bond distance of 1.3788 Å was derived. It deserves a special mention that geometry optimization at the CCSD(T) level for trimethylamine-*N*-oxide, **1**, gives a longer N–O bond distance of 1.372 Å (see also ESI†), which is closer to the experimental gas phase electron diffraction value of 1.379 Å.[7c] Since the QTAIM analysis for the MP2 and DFT derived electron densities revealed similar trends, we will focus exclusively on the discussion of the DFT results in the forthcoming text. Details of the corresponding MP2 calculations are found nevertheless in the ESI.†

For all amine-*N*-oxides **1–3**, a set of descriptors characterizing the pyramidality of the nitrogen atom, *i.e*. the out-of-plane deviation, POAV and pyramidality index, is essentially identical for both the experimental and computed geometries. This clearly suggests closely related electronic environments of the nitrogen atoms within the whole series.

Thus, neither the experimentally nor the theoretically derived geometrical parameters for the amine-*N*-oxides **1–4** could provide an explanation for the correlation of the calculated N–O bond dissociation enthalpies with the value x of the amine-*N*-oxides, $Ph_x(CH_3)_{3-x}N$–O. Therefore, we next turned to a closer inspection of the electronic nature of the N–O bond employing both experimental and theoretical topological analyses within the QTAIM approach.

Multipole refinement followed by full topological analysis for compound 2: experiment *versus* theory

For the amine-*N*-oxide, $Ph(CH_3)_2N$–O, we were able to carry out a comparative theoretical (DFT/PBE0) and experimental study of the electron density distribution $\rho(\mathbf{r})$ within the framework of QTAIM.[9] In both cases, (3, −1) bond critical points (BCPs) of $\rho(\mathbf{r})$ representing saddle points of the density distribution between bonded atoms were determined for all anticipated bonds, as well as the ring critical point (RCP, (3, +1)) corresponding to the phenyl ring (Fig. 4 and Table 2). It deserves a special mention that the BCP corresponding to the intramolecular C–H···O hydrogen bond between the oxygen atom and the ortho hydrogen atom of the phenyl ring

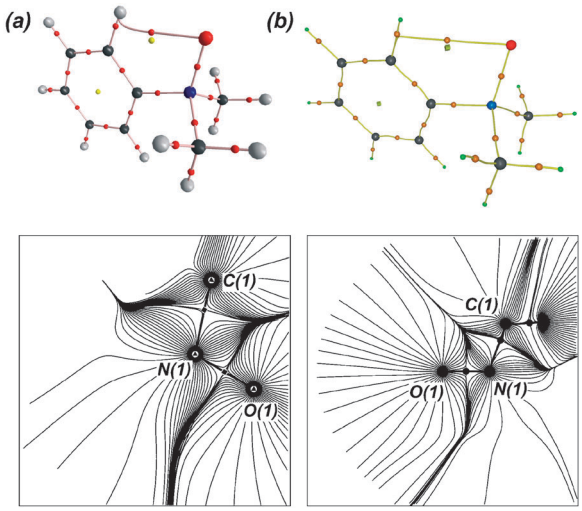

Fig. 4 Bond paths, critical points and trajectories (plane {O(1),N(1),C(1)}) for $Ph(CH_3)_2N$–O, **2**: (a) theoretical (DFT/PBE0) and (b) experimental.

was found in the theoretical and the experimental electron density distributions along with the corresponding RCP of the five-membered ring. The total number of critical points fulfills the Poincaré–Hopf equation and is therefore self-consistent.

The topological parameters for the BCP corresponding to the N–O bond show a good agreement of the experimental and theoretical data (Table 2). The bond order (n_{topo}) derived from the topological analysis[14] was found to be equal to 1.276 and 1.278 for the calculated and experimental data, respectively, and implies some extent of π-interaction (multiple bond character) contributing to the σ-type N–O single bond.

For the bond ellipticity (ε) of the N–O bond critical point, a value close to zero (Table 2) was derived from both, the experimental (ε = 0.0138) and computed electron density data (ε = 0.0081). These results suggest a rotationally symmetric ($\lambda_1 \approx \lambda_2$) electron density distribution and are characteristic for a single bond, as it is observed, for instance, at the BCP of the C–C single bond in ethane (ε = 0.0). The apparent inconsistency between the bond ellipticity and n_{topo} can be resolved considering the set of molecules used for the statistic fitting of the parameters a_0, a_1, a_2 and a_3 in Tsirelson's equation.[14] This fitting was mainly based on N–O bonds with bond orders higher than 1, such as in nitro-groups. It is therefore conceivable that these parameters might be ill-suited for the N–O bonds in amine-*N*-oxides and may lead to a systematic overestimation of the N–O bond order.

Next, we investigated the electron density ρ_b and the Laplacian function, L, ($L = -\frac{1}{4}\nabla^2\rho(\mathbf{r})$), at the N–O bond critical point of compound **2**. Positive values of the Laplacian function accompanied by high values of the electron density at the BCP are commonly associated with a distinct covalent character of the bond (so-called *shared interaction*), while highly negative values of the Laplacian function accompanied by relatively small values of the electron density are attributed to an ionic character of the (hydrogen) bonds, *i.e*. so-called *closed-shell interactions*.[15] It should be noted here that the Laplacian and Laplacian function have opposite signs. Hereafter, we mainly use the Laplacian for our discussion.

This journal is © the Owner Societies 2012

View Article Online

Published on 10 January 2012 on http://pubs.rsc.org | doi:10.1039/C2CP22341D
Downloaded by Universite de Picardie on 27 November 2012

Table 2 Selected experimental and theoretical topological parameters for the N–O bond in the amine-*N*-oxides considered

	Compound				
		$Ph(CH_3)_2N$–O, **2**			
Parameter	$(CH_3)_3N$–O, **1**	Exp.	Theor.	$Ph_2(CH_3)N$–O, **3**	Ph_3N–O, **4**
ρ_b[a]	0.367	0.346	0.371	0.368	0.363
$\nabla^2\rho_b$[b]	−0.28	−0.12	−0.30	−0.29	−0.26
λ_1[b]	−0.84	−0.77	−0.86	−0.85	−0.82
λ_2[b]	−0.84	−0.76	−0.85	−0.84	−0.82
λ_3[b]	1.41	1.41	1.41	1.41	1.40
$G(r_b)$[c]	0.21	0.21	0.21	0.21	0.21
n_{topo}[d]	1.26	1.23	1.28	1.26	1.25
$V(r_b)$[c]	−0.48	−0.45	−0.49	−0.48	−0.47
ε	0.00	0.01	0.01	0.01	0.00
$h(r_b)$[c]	−0.28	−0.24	−0.28	−0.27	−0.27
$\frac{G(r_b)}{\rho(r_b)}$[e]	0.56	0.61	0.56	0.56	0.57
$\frac{\lvert\lambda_1\rvert}{\lambda_2}$	0.60	0.54	0.61	0.61	0.59
$\frac{\lvert V(r_b)\rvert}{G(r_b)}$	2.34	2.13	2.36	2.35	2.30
$I(r_b) = \frac{h(r_b)}{\rho(r_b)}$[e]	−0.75	−0.69	−0.76	−0.75	−0.74
$q(N)$[f]	−0.43	−0.63	−0.39	−0.36	−0.37
$q(O)$[f]	−0.74	−0.68	−0.71	−0.70	−0.69

[a] In units of [e Bohr^{-3}]. [b] In units of [e Bohr^{-5}]. [c] In units of [Hartree Bohr^{-3}]. [d] In accordance with the formula proposed by Tsirelson *et al.*[14] [e] In units of [Hartree e^{-1}]. [f] In units of [e].

In the case of the amine-*N*-oxide, $Ph(CH_3)_2N$–O (**2**), the electron density and the Laplacian function (ρ_b(exp.) = 0.3451, ρ_b(calc.) = 0.3708; $\nabla^2\rho_b$(exp.) = −0.1090, $\nabla^2\rho_b$(calc.) = −0.2955) indicate that the N–O bond can be described as a σ-type covalent single bond. However, our detailed analysis of the kinetic, potential and total energy densities (Table 2) as well as the binding degree parameter (I_b), which are well-known to be sensitive to the nature of the bond,[15] point to a noticeable contribution of the closed-shell interaction. Thus, the N–O bond in compound **2** is best described as a *polar covalent bond*.

Furthermore, we investigated in detail the second derivative of the charge density distribution around the N–O bond for charge accumulation and depletion. Valence shell charge concentrations (VSCCs) were identified as (3, −3) critical points in the negative Laplacian (local maximum). The inspection of the 3D representation of the Laplacian (Fig. 5) reveals a quasi-toroidal topology around the oxygen atom arising from its lone pairs. Moreover, the 2D intersection map of the theoretical Laplacian (Fig. 5(a)) shows an important feature, *i.e.* a very thin neck corresponding to the N–O bond; in the experimental data this neck is not observed (Fig. 5(b)). It is instrumental to compare these features with the 2D map of a standard covalent bond of the neighboring C(1)–N(1) bond. Similar results for the Laplacian distribution were obtained in previous theoretical studies of H_3N–O and $(CH_3)_3N$–O.[16] These results unambiguously confirm an anionic character of the oxygen atom and a negligible participation of its lone pair in bonding with the nitrogen atom N(1). This conclusion is fully supported by calculation of the (QTAIM) charge for O(1) obtained by integration of the electronic density over the atomic basin, which amounts to *ca.* $q(O) \approx 0.7e$ for both experimental and theoretical data (Table 2).

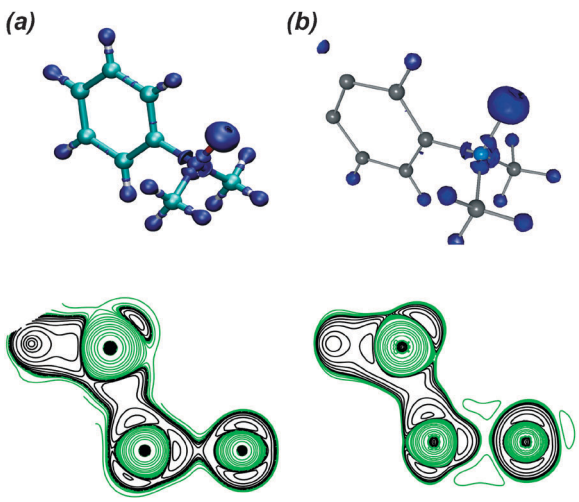

Fig. 5 3D maps and 2D intersections (plane {O(1),N(1),C(1)}) of both the theoretical and experimental Laplacian for $Ph(CH_3)_2N$–O, **2**: (a) theoretical and (b) experimental (green lines correspond to positive values, black lines to negative values).

Another important feature of the electronic structure of molecule **2** is the presence of an intramolecular hydrogen bond. The bond path corresponding to this hydrogen bond was observed for both the X-ray derived and calculated electron densities (Fig. 4). This type of bond represents an example of the classical C–H···O hydrogen bonding,[9b,17] which plays an important role in a variety of biological applications. It is frequently encountered in carbohydrates[18] and nucleosides[19] and the tertiary structure of macromolecules.[19] The topological parameters based on the electron density for the BCPs (ρ_b and $\nabla^2\rho_b$, Table 3) evidence closed-shell type

Published on 10 January 2012 on http://pubs.rsc.org | doi:10.1039/C2CP22341D
Downloaded by Universite de Picardie on 27 November 2012

Table 3 Selected experimental and theoretical parameters of the intramolecular hydrogen bonds in the phenyl substituted amine-*N*-oxides, **2** and **3**

	$Ph(CH_3)_2N$–O, **2**		$Ph(CH_3)_2N$–O, **3**
Parameter	Exp.	Theor.	Theor.
ρ_b[a]	0.018	0.023	0.023
$\nabla^2\rho_b$[b]	0.09	0.10	0.10
$G(r_b)$[c]	0.02	0.02	0.02
$V(r_b)$[c]	−0.01	−0.01	−0.01
$h(r_b)$[c]	0.01	0.01	0.01
$\frac{G(r_b)}{\rho(r_b)}$[d]	0.96	0.84	0.84
$\frac{\lvert V(r_b)\rvert}{G(r_b)}$	0.64	0.69	0.69
$I(r_b) = \frac{h(r_b)}{\rho(r_b)}$[d]	0.34	0.26	0.26
E(H-bond)/kcal mol^{-1}	−3.5	−4.1	−4.2

[a] In units of [e Bohr^{-3}]. [b] In units of [e Bohr^{-5}]. [c] In units of [Hartree Bohr^{-3}]. [d] In units of [Hartree e^{-1}].

interactions, while the analysis of potential, kinetic and total energy densities is indicative of an additional small covalent contribution. From a large set of hydrogen bonds (including classical O–H···O and O–H···N) one must conclude that C–H···O bonds are mostly weak but not invariably so.[17,20] The topological analysis of the electron density distribution function $\rho(\mathbf{r})$ derived from experimental data and *ab initio* calculations in conjunction with Espinosa's correlation scheme[21] makes it possible to estimate the interaction energy with reasonable accuracy.[22] The derived values for E(C–H···O) of −3.5(exp.) and −4.1(theory) kcal mol^{-1} in compound **2** show an excellent agreement and again confirm the high applicability of this theoretical model (Table 3). Moreover, these relatively high values document a rather strong intramolecular C–H···O hydrogen bond in the amine-*N*-oxide **2**.

Full topological analysis for the series of the $Ph_x(CH_3)_{3-x}N$–O amine-*N*-oxide molecules

The excellent agreement of the experimental and theoretical topological parameters for compound **2** prompted us to perform a full QTAIM analysis of the remaining amine-*N*-oxides **1**, **3** and **4** at the same level of theory (DFT/PBE0). We anticipated to gain further insights into the N–O bonding situation and, in particular, to shed some light on the correlation of the N–O bond dissociation enthalpies with the parameter x in the series of the amine-*N*-oxides **1–4**.

Selected topological parameters for the amine-*N*-oxides **1**, **3** and **4** are presented in Table 2. For all compounds the Poincaré–Hopf requirement is fulfilled. The distributions of the electronic density ($\rho(\mathbf{r})$) as well as trajectory plots ($\nabla\rho(\mathbf{r})$) reveal a high similarity for all molecules considered (Fig. 4 and 6). The N–O bond orders (n_{topo}) for the amine-*N*-oxides **1**, **3** and **4** fall into the range of 1.25–1.27 indicating only negligible changes in the bond nature in going from $(CH_3)_3N$–O (**1**) to Ph_3N–O (**4**). The corresponding N–O bond ellipticities were found to be very close to 0 evidencing a rotational symmetry of the charge distribution ($\lambda_1 \approx \lambda_2$), *i.e.* consistent with the anticipated N–O σ-bond. The BCPs of the N–O bonds are characterized by high values of the electronic density function $\rho(\mathbf{r})$ and negative values of the Laplacian (Table 2) suggesting a covalent bond, whereas the analysis of energy density parameters evidences noticeable contribution of closed-shell (ionic) interactions.

These findings completely agree with the experimental data obtained for compound **2**. The observation of only slight changes of the topological descriptors in the series should be especially underlined. The anionic character of the oxygen atoms in the amine-*N*-oxides was unambiguously evidenced by analysis of the Laplacian (Fig. 5 and 6) as well as the QTAIM atomic charges. In summary, this corroborates that *there are no significant differences in the nature* and, as consequence, *the stability of the N–O bond* in going from **1** to **4**. Hence, the QTAIM analysis implied that the calculated trend of bond dissociation enthalpies in this series (Fig. 1) were due to electronic/structural changes between the amine-*N*-oxides and their corresponding amines.

It is noteworthy that the X-ray crystal structure of $Ph_2(CH_3)N$–O, **3**, also revealed intramolecular C–H···O hydrogen bonding of one phenyl hydrogen atom (Fig. 3). The calculated equilibrium geometry for this molecule also displays two inequivalent phenyl groups with corresponding dihedral angles ($\angle$ O(1)–N(1)–C(3)–C(4)) of 4.8° (ring I) and 43.7° (ring II). The presence of a bond path between the oxygen atom and an ortho hydrogen atom of (only) one of the phenyl rings (ring I) clearly confirmed the existence of a C–H···O hydrogen bond. The absence of another hydrogen bond to the second ring makes the two phenyl substituents inequivalent and, subsequently, leads to two isomers (enantiomers) for compound **3** in the solid state. The topological parameters at the H···O BCP in **3** are comparable with the corresponding values found for the amine-*N*-oxide **2** (Table 3). The rules for this type of closed-shell interactions with small covalent contributions are fulfilled.[15] The almost identical values for the C–H···O hydrogen bonding energy of −4.2 kcal mol^{-1} for $Ph(CH_3)_2N$–O (**2**) and −4.1 kcal mol^{-1} for $Ph_2(CH_3)N$–O) (**3**) are remarkable. In order to gain further insight into the energetics of these interactions, Walsh diagrams for the rotation around the N(1)–C(1) bond were calculated (Fig. 7).

Inspection of Fig. 7 revealed for both amine-*N*-oxides **2** and **3** energy minima at dihedral angles of approximately 0°. When this torsion angle is increased, the energy rises and reaches a maximum at angles of 90° for **2** and 70° for **3**. Based on the O···H distance of 3.30 Å and 2.90 Å of the ortho-hydrogen atom of the phenyl ring and the oxygen atom in **2** and **3**, it is anticipated that hydrogen bonding is absent at these maxima. The intramolecular hydrogen bonding strengths were estimated from the energy differences of the minima and maxima. The derived values of 5.4 kcal mol^{-1} and 2.0 kcal mol^{-1} for **2** and **3**, respectively, are in reasonable agreement with the results obtained in the topological analysis (Table 3: **2**: 4.2, **3**: 4.1 [kcal mol^{-1}]). The lower value for compound **3** is explained by compensation of the diminishing hydrogen bond through the (incipient) formation of another C–H···O bond to the other ring due to a correlated rotation of the phenyl rings. Hence, in the energetic minimum of **3**, only *one* phenyl C–H-bond is involved in intramolecular hydrogen bonding. Interestingly, the geometry optimized structure of the fully phenyl substituted amine-*N*-oxide,

 This journal is © the Owner Societies 2012

Published on 10 January 2012 on http://pubs.rsc.org | doi:10.1039/C2CP22341D
Downloaded by Universite de Picardie on 27 November 2012

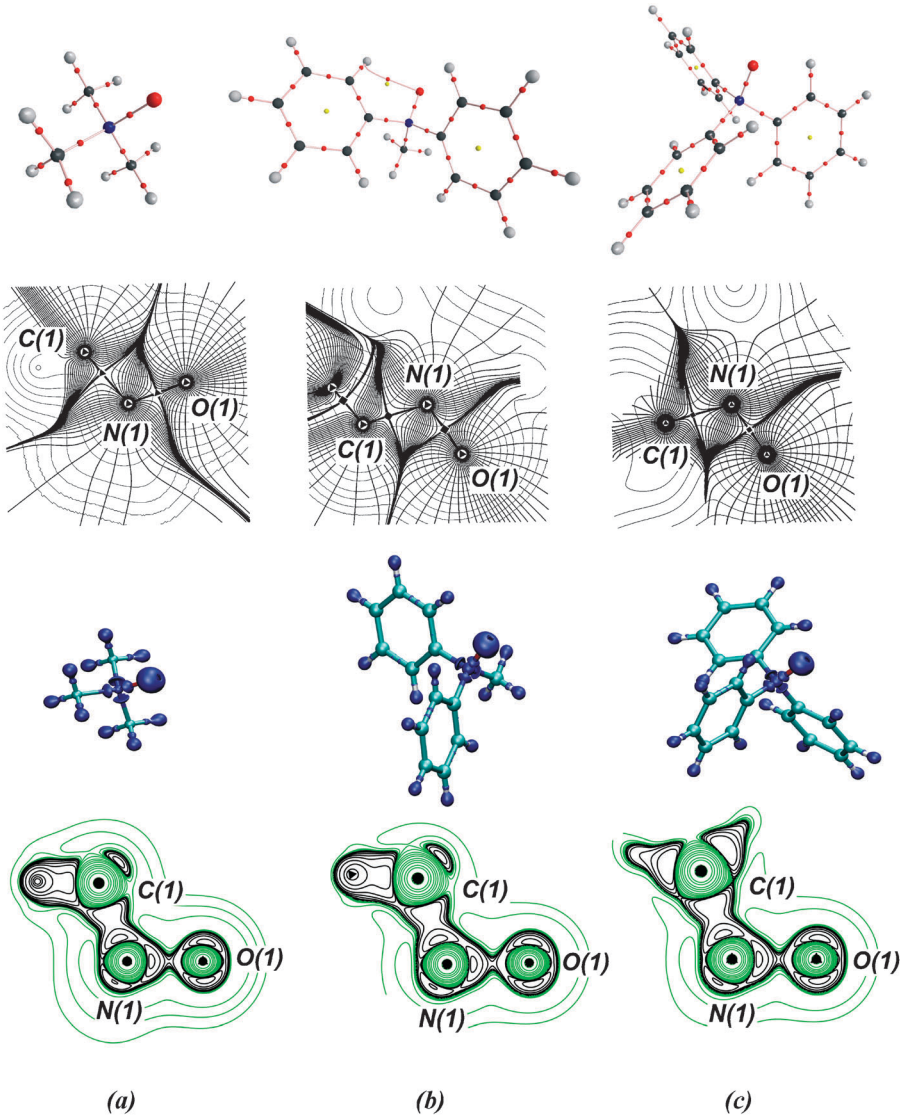

Fig. 6 Bond paths, trajectories, 3D maps of the Laplacian and corresponding 2D intersections (plane {C(1),N(1),O(1)}) of $\nabla^2\rho(\mathbf{r})$ for: (a) $(CH_3)_3N$–O (**1**), (b) $Ph_2(CH_3)N$–O (**3**) and (c) Ph_3N–O (**4**).

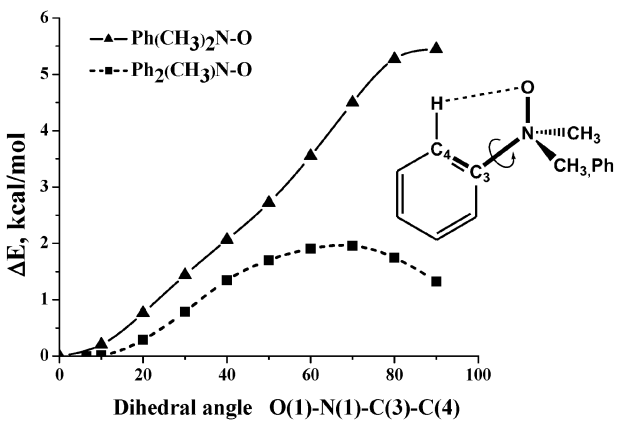

Fig. 7 Walsh diagram for rotation around the N–C_{Phenyl} bond in $Ph(CH_3)_2N$–O (**2**) and $Ph_2(CH_3)N$–O (**3**). The constrained dihedral angle is highlighted in bold in the inset.

Ph_3N–O (**4**), displays no intramolecular hydrogen bonds. This is presumably due to the sterical hindrance, which leads to the preferred propeller shaped arrangement of the phenyl rings.

NBO analysis of the $Ph_x(CH_3)_{3-x}N$–O molecules

The topological analysis of the calculated and experimental electron densities pointed toward structural/electronic changes between the amine-*N*-oxides and their corresponding amines as source for the trend of the stability of the N–O-bonds. We have nevertheless included natural bond orbital (NBO) analysis[23] for the amine-*N*-oxides series **1–4**, since this technique was previously employed with success to elucidate details of the electronic structure of the parent amine-*N*-oxide, H_3N–O[24] (see ESI†, for details).

The natural bond orbitals (NBOs) correspond to >99% of the corresponding natural localized MOs (NLMOs) and are thus appropriate for the analysis of the N–O bonding situation

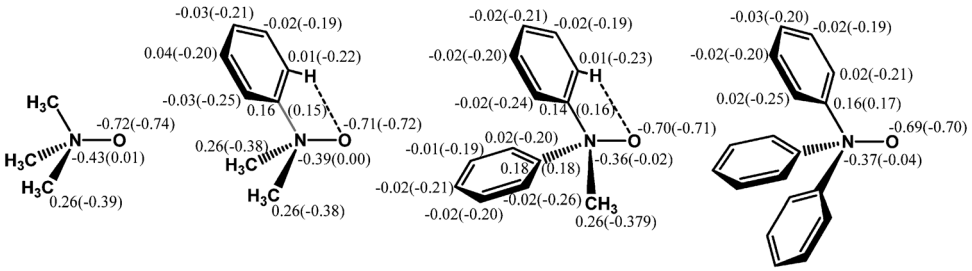

Fig. 8 DFT/PBE0 based QTAIM and NBO (in parentheses) charge distributions of the heavy atoms in the amine-*N*-oxides **1–4**. For the C_3-symmetrical compounds **1** and **4** only the charges of one methyl group or ring are shown.

Published on 10 January 2012 on http://pubs.rsc.org | doi:10.1039/C2CP22341D
Downloaded by Universite de Picardie on 27 November 2012

in the amine-*N*-oxides **1–4** (for a set of orbitals in the frame of an NBO technique at different levels of localization, see ESI†). Importantly, the N–O bond order is very similar for all amine-*N*-oxide compounds of the series and corresponds to a single bond. This is in a good agreement with the results of the topological analysis of the experimental and calculated electron densities (*vide supra*). The composition of the NBOs for the whole series reveals that the electron density of the N–O bond is predominantly provided by the nitrogen atom. In terms of NBO, the N–O bond is formed by overlap of the natural hybrid orbitals (NHOs) of the oxygen (~45%) and nitrogen (~55%) atoms. Interestingly, the contribution of s-type atomic orbitals to the NHO is noticeably larger for nitrogen (~26%) than for the oxygen atom (~17%).

The charge distributions in all molecules of the series are depicted graphically in Fig. 8 for both AIM and NBO (NPA) derived charges. The high negative charge of the oxygen atoms of *ca.* −0.7*e* for all amine-*N*-oxides should be especially underlined, which is observed for both the NBO and AIM charges. A good agreement between both methods is also observed for the charges of the ipso-carbon atoms in the phenyl substituted amine-*N*-oxides **2a–4a**, which display essentially identical positive values of +0.16*e* for both the NPA and AIM charges. There is however a notable difference of the NPA and AIM charges for the residual parts of the molecules. While the NBO analyses reveal NPA charges for the nitrogen atoms close to 0, the AIM charges display significantly negative values of *ca.* −0.4*e*. A reversal of the charges for both methods is also noticed for the methyl groups for which negative NPA charges of *ca.* −0.4*e* were derived. This in sharp contrast to the positive values of +0.26*e* for the AIM charges for all methyl groups in the amine-*N*-oxides **1–3**. Furthermore, the AIM charges of the residual (*ortho*, *meta* and *para*) carbon atoms of the phenyl rings in **2–4** are close to zero, while the NPA charges for these residual carbon atoms amount to *ca.* −0.2*e*.

Despite these apparent differences of the AIM and NPA charges both methods clearly reveal a polar N–O bond in the amine-*N*-oxides **1–4** with a delocalized charged distribution, which is significantly more pronounced in the NBO data.

Overall, the results of the NBO analysis are thus in agreement with the QTAIM analysis and are fully consistent with a polar, covalent N–O σ-bond in the amine-*N*-oxides, *i.e.* with a $Ph_x(CH_3)_{3-x}N^{\delta+}$–$O^{\delta-}$ valence bond structure. Moreover, the comparison of the NBO parameters compiled for **1–4** suggests a closely related N–O bonding situation in all amine-*N*-oxides of the series. This contrasted the strong variation of the corresponding bond dissociation enthalpies in **1–4** (Fig. 1) and thus provided further evidence that the N–O bond strengths in the amine-*N*-oxides are not dominated by their ground states but rather electronic/structural differences between the amines and their corresponding *N*-oxides. The final piece of evidence in support of this view was provided by multireference calculations, which are reported in the next section.

Ground state and bond dissociation enthalpy (BDE): multireference CASSCF(6,6) and subsequent MCQDPT2 calculations

Ground state properties. In search for an explanation of the noticed trend of the BDEs for the N–O bonds in compounds **1–4**, we turned to high-level multireference CASSCF(6,6) calculations.

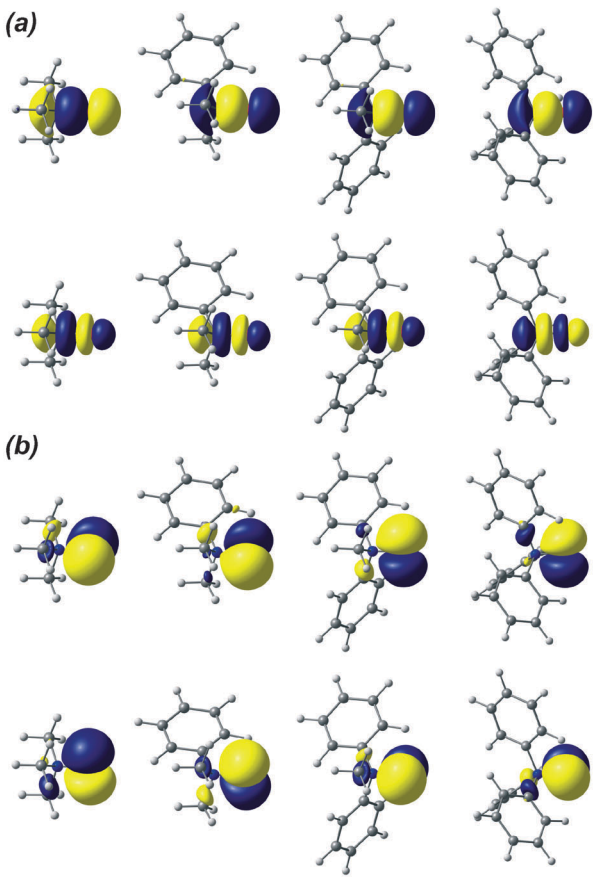

Fig. 9 Natural orbitals for $Ph_x(CH_3)_{3-x}N$–O: (a) corresponding to bonding and anti-bonding situations of the N–O bond and (b) corresponding to the lone pairs of the oxygen atom (most left: **1**; second left: **2**, second right: **3**, most right: **4**).

This journal is © the Owner Societies 2012

Published on 10 January 2012 on http://pubs.rsc.org | doi:10.1039/C2CP22341D
Downloaded by Universite de Picardie on 27 November 2012

First, the multireference character of the wavefunctions for all *N*-oxides was analyzed. The main electronic configuration was found to be $\sigma^2\pi_1{}^2\pi_2{}^2\sigma^{*0}\pi_1{}^{*0}\pi_2{}^{*0}$ with a weight of >96% for all molecules of the series. This justified the application and results based on our single reference DFT calculations. The analysis of the natural orbitals (Fig. 9) corroborated our previous description of the N–O bonds in the amine-*N*-oxides as isolated (single) σ-bonds, since we could neither find significant contributions from the lone pairs localized on the oxygen atom nor from the amine parts of the molecules. The occupation of the natural orbitals corresponding to the N–O bond was found to be very close to 2 for all compounds **1–4**. The calculated N–O bond order based on the population of the bonding and anti-bonding NOs[25] is equal to 0.968 ± 0.001 for all amine-*N*-oxides and provided further evidence for N–O single bonds in all molecules of the series.

The natural orbitals corresponding to the lone pairs of the oxygen atom revealed well-shaped p-orbitals in all amine-*N*-oxides **1–4** (Fig. 9, entry (*b*)). The populations of the p-orbitals of the oxygen atoms are equal to 4.659, 4.676, 4.686 and 4.710 for **1**, **2**, **3** and **4**, respectively, and clearly show the anionic character of the oxygen atom with a noticeable electron transfer (∼0.6–0.7*e*) from the nitrogen atom. This sizeable charge accumulation at the oxygen atom is in agreement with the results of single-reference calculations (*vide supra*).

The significant anionic character of the oxygen atoms in these systems leads to formation of strong hydrogen bonds networks when placed in polar protic solvents such as water. It was previously confirmed in several studies that trimethylamine-*N*-oxide, **1**, affects the folding of biomolecules *via* strong hydrogen bonds network in aqueous media involving several molecules of water.[5] There is a small albeit notable increase of the populations of the p-orbitals of the oxygen atom with an increasing number of the phenyl groups, which could lead to even stronger hydrogen bonding in such systems. This point will be addressed by us in a forthcoming study.

Bond dissociation energy. The CASSCF(6,6) analysis of the electronic structure of the amine-*N*-oxides revealed so far no reason for the strong dependence of the BDE on the number of phenyl substituents. The logical next step was therefore to focus on the energetics of the N–O bond dissociation process. Taking into account the triplet ground state of the formed oxygen atom, crossing along the potential energy surfaces corresponding to singlet and triplet pathways, *i.e.* (i) $^1R_3N{-}O \rightarrow {}^1R_3N + {}^1O$ and (ii) $^1R_3N{-}O \rightarrow {}^1R_3N + {}^3O$ is likely to occur. The use of multireference approaches such as CASSCF and, preferably, subsequent multireference perturbation theory was therefore deemed necessary.

For the calculations of the bond dissociation energies, the non-size-consistent behavior of both, the CASSCF and MR-perturbation theory, had to be addressed appropriately. The bond dissociation energy was estimated as the difference between the calculated absolute energies of the amine-*N*-oxide and, of a system, where the oxygen atom was moved away from the residual amine fragment by a large distance (>10 Å, *cf.* ESI†). Both the aforementioned singlet (i) and triplet (ii) N–O bond dissociation pathways were initially considered.

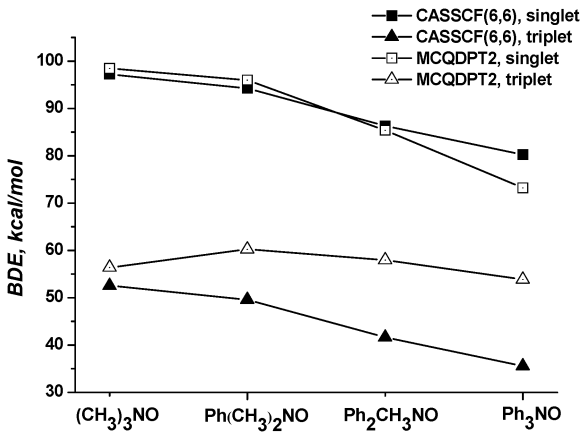

Fig. 10 Comparative diagram for the dependence of the BDE values on the number of phenyl substituents in $Ph_x(CH_3)_{3-x}N{-}O$ for both, the singlet and triplet dissociation pathways at the CASSCF(6,6) and the MCQDPT2 levels of theory.

The calculations clearly supported the strong preference of the triplet N–O bond dissociation pathway (ii) (Fig. 10). Keeping in mind that atomic oxygen has a triplet ground state, these results were expected. Hence, hereafter only the triplet pathway will be considered for the discussion of the N–O bond dissociation energies. It deserves a special mention that in spite of the tendency that absolute bond dissociation energies are in general well reproduced in CASSCF calculations, the differences in the N–O bond energies obtained at the CASSCF and DFT levels for all amine-*N*-oxides **1–4** are substantial. In fact, in comparison with the DFT calculations (vide supra) we had to witness a weakening of *ca.* 17 kcal mol^{-1} of the N–O bond dissociation energies at the CASSCF level. This apparent mismatch could be cured by the incorporation of dynamic electron correlation, which was made available through second-order perturbation calculations at the MCQDPT2 level on top of the CASSCF reference wavefunctions.

Special attention has to be drawn to the trend of the N–O BDEs for the series of different amine-*N*-oxides calculated at the MCQDPT2 level (Fig. 10). In sharp contrast to the previous DFT calculations these values appeared to be essentially *invariant* with regard to the number of phenyl substituents *x*! This apparent disparity could be quickly resolved and provided the *final evidence* to explain the observed trend of BDEs of the N–O bonds in the amine-*N*-oxide. In contrast to the DFT calculations, we had (initially) refrained from the re-optimization of the free amines formed in the dissociation process for the sake of saving computational time. This clearly showed that changes of the geometrical environment at the nitrogen atoms in the course of the N–O bond rupture, *i.e.* geometry relaxations, dominate the N–O bond strengths. It should be noted that previous energy decomposition analyses of bond energies by several groups revealed similar results for various molecular systems.[26]

Influence of the geometry relaxation

The relevance of geometry relaxation for the N–O bond strength is best illustrated by comparison of the X-ray structural data for triphenylamine, **4a**, and the computed structure of the

Published on 10 January 2012 on http://pubs.rsc.org | doi:10.1039/C2CP22341D
Downloaded by Universite de Picardie on 27 November 2012

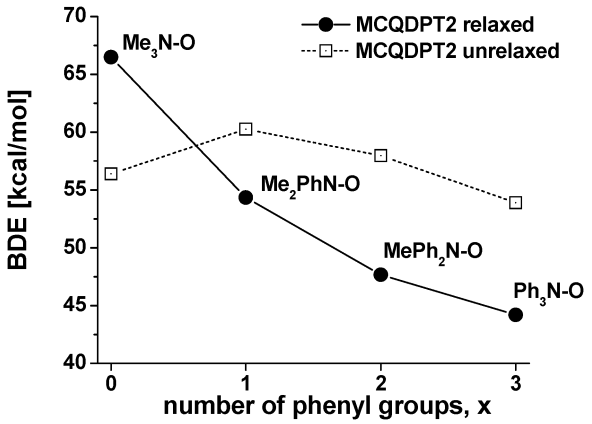

Fig. 11 Trend of the N–O bond dissociation enthalpies in the amine-*N*-oxides **1–4** for "relaxed and unrelaxed" geometries of the amine products.

corresponding amine-*N*-oxide **4**. While the free amine displays a trigonal planar geometry of the nitrogen atom (*cf.* below),[27] it has to undergo a significant tetrahedral distortion during formation of its corresponding amine-*N*-oxide **4**. The DFT optimized geometry of the latter indicates a nearly ideal tetrahedral environment of the nitrogen atom, which is corroborated from the related ∠C–N–C and ∠C–N–O bond angles of 109.7° and 109.2°, respectively. In our initial MCQDPT2 calculations, we had obviously not considered this type of distortion in the direction of **4** → **4a** or relaxation in going from **4a** → **4**.

In order to include the influence of the geometry relaxation at the MCQDPT2 level, we repeated these calculations albeit with the following changes: For the calculation of the total energy of the product side, the DFT optimized structures of the free amines were now employed and the oxygen atom was placed 10 Å apart from the nitrogen atom as denoted before. From these calculations, relaxation corrected N–O bond energies were obtained, which are presented graphically in Fig. 11 for the series of amine-*N*-oxides **1–4**.

In contrast to the nearly constant N–O bond dissociation enthalpies (55–50 kcal mol^{-1}) when geometry relaxation of the formed amines was disregarded, the data depicted in Fig. 11 clearly show that the calculated values at the MCQDPT2 level including geometry relaxation reflect the same trend previously observed in the DFT calculations. These can be envisaged regarding the N–O bond dissociation enthalpy of 65 kcal mol^{-1} in **1**, which dropped to *ca.* 45 kcal mol^{-1} in Ph_3N–O, **4**. It should be noted in passing that the calculated BDE for the N–O bond in trimethylamine-*N*-oxide, **1**, is in excellent agreement with the experimental value of 60 kcal mol^{-1}.[5]

Most notably, these calculations provided the final piece of evidence that the energetics of the N–O bonding situation in **1–4** are dominated by the relaxation energy, respectively, the preparation energy ΔE_{prep} for the reverse bond forming process. This prompted us to investigate the corresponding amines **1a–4a** in some detail (Fig. 12).

Theoretical investigation of the parent amines 1a–4a

Before the electronic structure of the amines **1a–4a** will be discussed in some detail, the trend observed for their pK_b values and gas phase proton affinities deserves a special mention. The basicity of **1a–4a** and the closely related (protio) amines[28] shown in Fig. 13 (left) displays a strong resemblance with the linear dependence of the N–O bond dissociation enthalpies in the amine-*N*-oxides **1–4** on the number of phenyl groups (*cf.* Fig. 2). It is interesting to note that the gas phase proton affinities for the same series of protio amines (Fig. 13, right) display a reverse trend of the basicity, *i.e.* in contrast to the behavior in solution, triphenylamine, Ph_3N, is a stronger base than ammonia! For the series **1a–4a** on the other hand,

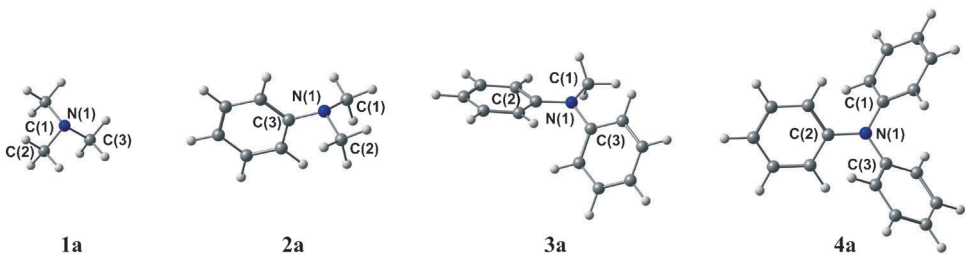

Fig. 12 Geometry optimized structures (DFT/PBE0) of the parent amines, $Ph_x(CH_3)_{3-x}N$, **1a–4a**, along with the labeling scheme.

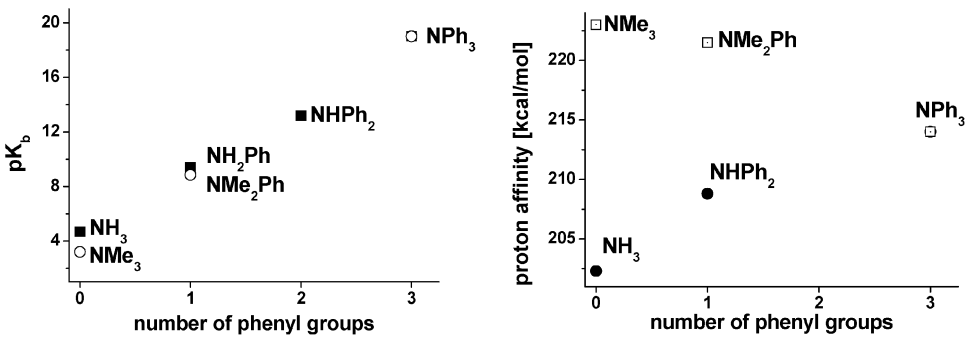

Fig. 13 Dependence of the pK_b values (left) and proton affinities (right) on the number of phenyl groups for a series of amines (based on data reported in ref. 28).

 This journal is © the Owner Societies 2012

Published on 10 January 2012 on http://pubs.rsc.org | doi:10.1039/C2CP22341D
Downloaded by Universite de Picardie on 27 November 2012

Table 4 Selected geometrical parameters for the (DFT/PBE0) optimized structures of the amines, $Ph_x(CH_3)_{3-x}N$ (x = 0–3), **1a–4a**; distances are given in [Å], angles in [°]

	Compound			
Parameter	$(CH_3)_3N$ **1a**	$Ph(CH_3)_2N$ **2a**	Ph_2CH_3N **3a**	Ph_3N **4a**
N(1)–C(1)	1.443	1.449	1.445	1.409
N(1)–C(2)	1.443	1.449	1.393	1.409
N(1)–C(3)	1.443	1.432	1.411	1.409
Out-of-plane position of N(1)[a] [Å]	0.437	0.398	0.141	0
POAV (N)	107.6	106.2	95.6	90.1
Pyramidality index	0.71	0.66	0.25	0.01

[a] Plane spanned by the three nitrogen bonded carbon atoms.

the proton affinity decays when the number of phenyl groups is increased. This is in perfect agreement with the predicted trend of N–O bond dissociation enthalpies in the amine-*N*-oxides **1–4** (Fig. 2).

The comparison of the DFT optimized structures of the amine series **1a–4a** presented in Fig. 12 with available X-ray crystallographic[27,29] and gas phase electron diffraction data[30] revealed a very good agreement. Within the series, the trend of the POAVs of 107.6° (**1a**), 106.2° (**2a**), 95.57° (**3a**) and 90.1° (**4a**) indicates a neat transition from an almost tetrahedral structure of $(CH_3)_3N$, **1a**, to the trigonal planar environment of the nitrogen atom in Ph_3N, **4a** (Table 4). The latter is consistent with previous extensive experimental[27,30,31] and theoretical[31f,32] studies of **4a** suggesting a three-bladed propeller structure for the molecule with a planar or nearly planar central NCCC moiety. As for the POAVs, the same tendency was also observed for the pyramidality indexes and for the out-of-plane deviations of the nitrogen atoms (Table 4).

Obviously, pyramidalization of the nitrogen atom is a prerequisite to form the N–O bond in the amine-*N*-oxide. For the planar triphenylamine, **4a**, a geometrical change at the nitrogen atom with concomitant substantial preparation energy, ΔE_{prep}, is therefore required in the course of the formation of **4** from **4a**. For the pyramidal trimethylamine, **1a**, on the other hand, only small geometric adjustments with a small preparation energy were anticipated in going from **1a** → **1**. We addressed the energetics of the pyramidalization process through DFT calculations, which revealed an inversion barrier of *ca.* 5 kcal mol^{-1} for trimethylamine, **1a** (Fig. 14, left). This is consistent with recent calculations at the MP4 level[33] and experimental data for this process for **1a** and suggested a negligible preparation energy ΔE_{prep}.

As anticipated, the planar structure with a sp^2-hybridized nitrogen atom is favored in triphenylamine **4a** and a value of *ca.* 10 kcal mol^{-1} for ΔE_{prep} is required to distort to the pyramidal geometry observed in the corresponding amine-*N*-oxide **4**. Together with the data of the theoretical and experimental study of the *N*-oxides presented above, these results fully support the following explanation: the alternation in the N–O bond dissociation enthalpy in **1–4** is almost exclusively due to the difference in the preparation energy of the corresponding amines **1a–4a**.

Additional support for this conclusion comes from the previously published experimental results for azatriptycene and its isolated (!) corresponding amine-*N*-oxide.[34] The latter is shown below,

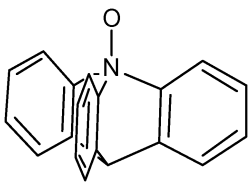

and is a congener of triphenylamine-*N*-oxide **4**. Due to ring constraints however, the amine (azatriptycene) displays a pyramidal geometry – in sharp contrast to the planar structure of triphenylamine, **4a**! Therefore, there is only negligible relaxation energy ΔE_{prep} in going from the azatriptycene-*N*-oxide to its amine, which is nicely reflected in the DFT/PBE0 estimated N–O bond energy according to eqn (1). The latter revealed a value of ΔE = −9.3 kcal mol^{-1} for the dissociation of the amine-*N*-oxide to the amine and $\frac{1}{2}$ equivalent $^3O_2$ for this system comparing well to the energetics of the amine-*N*-oxide **2**, $MePh_2N$–O (ΔE = −6.9 kcal mol^{-1}) rather than to the values for **4**, Ph_3N–O (ΔE = −27.8 kcal mol^{-1}).

The aforementioned geometrical distortions and the corresponding preparation energies can be easily connected with changes of the electronic structure, *e.g.* the dipole moment. In fact, the dependence of the dipole moment on the extent of pyramidalization for trimethylamine and triphenylamine is strongly opposite to the changes of the relative energies

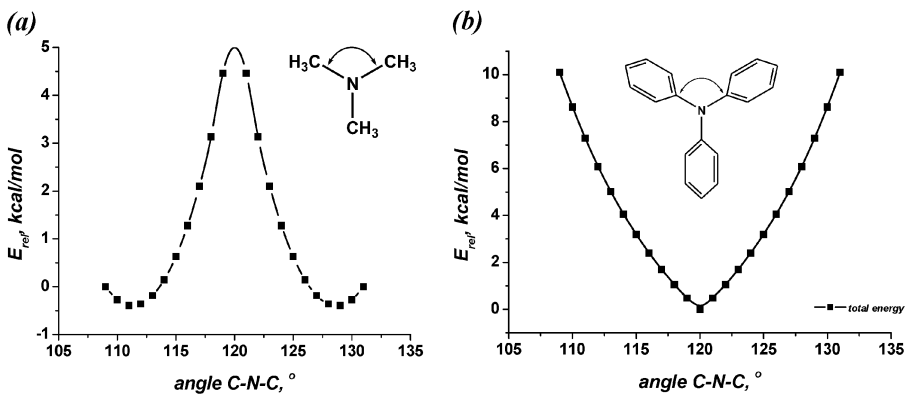

Fig. 14 Dependence of the relative energies on the pyramidality of the nitrogen atom in the amines **1a** (a) and **4a** (b).

Published on 10 January 2012 on http://pubs.rsc.org | doi:10.1039/C2CP22341D
Downloaded by Universite de Picardie on 27 November 2012

Table 5 Selected parameters related to the electronic structure of the amines $Ph_x(CH_3)_{3-x}N$ (**1a–4a**) and NH_3

Parameter	NH_3	$(CH_3)_3N$ **1a**	$Ph(CH_3)_2N$ **2a**	$Ph_2(CH_3)N$ **3a**	Ph_3N **4a**
q(N)	−1.041	−0.514	−0.529	−0.474	−0.482
D, Db	1.53	0.56	0.398	0.141	0.000
Configuration (N)	$s^{1.50}p^{4.19}$	$s^{1.27}p^{4.22}$	$s^{1.27}p^{4.22}$	$s^{1.18}p^{4.26}$	$s^{1.16}p^{4.28}$
$\Sigma(\Delta E^{(2)})$/kcal mol^{-1}		35.7	38.4	75.0	85.5
$\Delta E^{(2)}_{\text{methyl}}$/kcal mol^{-1}		11.9	12.3	12.5	
$\Delta E^{(2)}_{\text{I phenyl}}$, kcal mol^{-1}			13.8	24.6	28.5
$\Delta E^{(2)}_{\text{II phenyl}}$, kcal mol^{-1}				37.9	28.5

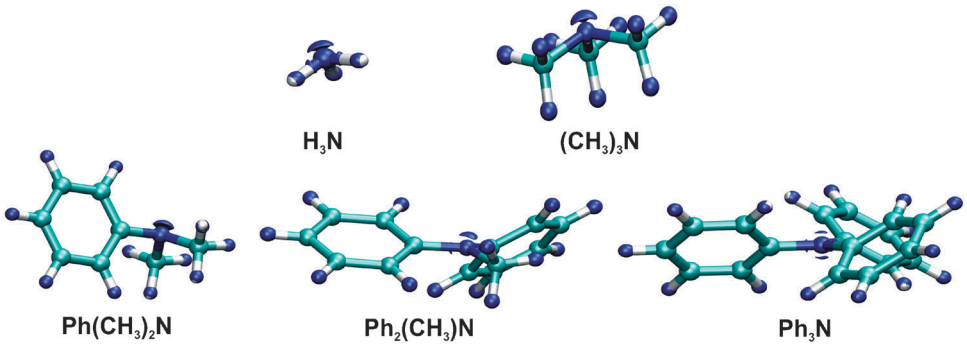

Fig. 15 3D maps of the charge concentrations ($\nabla^2\rho(\mathbf{r})$) for the tertiary amines **1a–4a** and NH_3 (isosurface value: −1.32 a.u.).

(*cf.* Fig. 14 and ESI†). In the series of amines considered the dipole moment smoothly decreases from **1a** to **4a** (Table 5). It can be interpreted in terms of localization/delocalization of the lone pair of the nitrogen atom when going from **1a** to **4a**. Larger tetrahedral distortion causes greater localization of the lone pair of the nitrogen and, consequently, an increase of the dipole moment.

This conclusion was confirmed by a set of topological descriptors such as the Laplacian, the one electron potential (OEP)[35] and the electron localization function (ELF)[36] applied to the amines **1a–4a** and also for ammonia, which was included for comparison (see ESI† for details). Special attention was paid to the distribution of the Laplacian and the related OEP, the functions describing the charge concentration region.[9,35] 3D maps of $\nabla^2\rho(\mathbf{r})$ for ammonia and the amines **1a–3a** unambiguously revealed the expected localization of the lone pair at the nitrogen atom (Fig. 15). Indeed, there is only one (−3,3) critical point in the distributions of the Laplacian and the OEP, which is a function homomorphous to $\nabla^2\rho(\mathbf{r})$.

This is a well-established behaviour of $\nabla^2\rho(\mathbf{r})$ for aliphatic amines[37] and has experimental support for tri-isopropylamine, $(i\text{-Pr})_3N$, from a precision high-angle X-ray experiment with subsequent multipole refinement.[38] In contrast, two equivalent (−3,3) CPs were found for triphenylamine, **4a**, indicating a strong delocalization of the nitrogen lone pair. A similar behavior was observed for the ELF. The volumes of the monosynaptic basins corresponding to the lone pairs of the nitrogen atoms decrease in going from NH_3 to $Ph_2(CH_3)N$. By contrast, two equivalent monosynaptic basins were observed at the nitrogen atom for Ph_3N, **4a**. All together, these topological techniques clearly point toward sp^2-hybridization of the nitrogen atom in **4a** (see also ESI†).

The reason for the localization/delocalization in the series **1a–4a** can be identified with the aid of the NBO technique, which was shown to be a very useful tool for the analysis of hyperconjugation effects in amines.[23a,39] In terms of the NBO methodology, hyperconjugation effects were described as electron transfer between the lone pair of the nitrogen atom (donor) and σ*(C–C) and/or π*(C–C) orbitals (acceptor) of the substituents. The extent of hyperconjugation can be easily monitored by the analysis of the occupancy, n(N), of the NBO corresponding to the nitrogen lone pair. In the series **1a–4a**, the values for n(N) decrease from 1.87 (**1a**) and 1.88 (**2a**) to 1.74 (**3a**) and 1.72 (**4a**) thereby evidencing an increase for this type of hyperconjugation in going from **1a** → **4a**. Interestingly, for ammonia the occupancy of the appropriate NBO is equal to 2.00. As anticipated the anti-bonding NBOs of π*(C–C)-type located on the phenyl substituents play a key role for this increase of delocalization (see for details ESI†). Energetically, these interactions can be quantified with help of the second-order perturbation theory in the NBO basis ($\Delta E^{(2)}$, Table 5). The values of $\Delta E^{(2)}$ dramatically increase from $(CH_3)_3N$ (35.7 kcal mol^{-1}) to Ph_3N (85.5 kcal mol^{-1}), which is mainly due to n(N) → π*(C–C) delocalization interactions.

The increased hyperconjugation effects in the series **1a** → **4a** stabilize the flattening of the amines in this order and lead therefore to larger values of ΔE_{prep} for amines with a larger number of phenyl groups. Thus, the analysis of the electronic structure and energetics of the parent amines **1a–4a** revealed the clear origin for the calculated trend of the preparation energies, which is required for the formation of the N–O bonds in the corresponding amine-*N*-oxides **1–4**. These findings provide an excellent fit of the dependence of N–O BDEs on the parameter x in the series **1–4**.

Conclusions

In the present study, a comprehensive theoretical analysis of the N–O bonding situation in a series of amine-*N*-oxides **1–4** was performed at different levels of theory. Based on consistent

 This journal is © the Owner Societies 2012

Published on 10 January 2012 on http://pubs.rsc.org | doi:10.1039/C2CP22341D
Downloaded by Universite de Picardie on 27 November 2012

results obtained by topological approaches (QTAIM), single-reference DFT methods and also highly-correlated multi-reference technique (MCQDPT2), the N–O bond in the amine-N-oxides **1–4** can be unanimously described as polar covalent σ-bond, *i.e.* a $Ph_x(CH_3)_{3-x}N^{\delta+}$–$O^{\delta-}$. In addition, the applied theoretical methodologies reveal that the nature of this bond is essentially independent on the number of phenyl substituents *x*. This conclusion was clearly supported by precision high-angle X-ray experiments followed by multipole refinement and the topological analysis of the experimental electron density for compound **2**.

The disparity of the unchanged N–O bond nature in **1–4** and the almost linear dependence of the BDEs on the number of phenyl groups *x* in the series of the amine-*N*-oxides can be explained superbly by the changes of the relaxation energies or preparation energies ΔE_{prep} in the reverse bond forming process from the corresponding amines **1a–4a**. The importance of this energetic term of the amines for the correct estimation of the chemical bond dissociation enthalpy was especially underlined. The origin of the trend in the preparation energies for the amines **1a–4a** was computationally analyzed in detail and was found to arise mainly from $n(N) \rightarrow \pi^*(C–C)$ delocalization interactions, which dramatically increase in the series **1a** → **4a**.

Thus, our study indicates that amine-*N*-oxides of the type $Ph_x(CH_3)_{3-x}N$–O represent a class of compounds with essentially identical electronic features of a specific bond albeit *different* bond dissociation energies. This type of behavior is met for instance in the observed trend of weaker dissociation enthalpies for the series of primary, secondary and tertiary alkyl C–H bonds, which are dominated by the stability of the corresponding carbon centered radicals.[40] It is deemed very instructive to recall this principle for the research community for other bonding studies, *e.g.* amine-*N*-oxides, where frequently (almost) exclusive attention is paid to the nature of the target bond.

Experimental and computational details

Experimental

The synthesis of compounds **2** and **3** was carried out according to the literature[41] by oxidation of the corresponding tertiary amines with *m*-chloroperbenzoic acid (for details see ESI†).

Routine X-ray experiments followed by spherical atom refinement

Crystals of **2** and **3** suitable for X-ray experiments were grown by slow evaporation of the solvent from an acetone/pentane (1 : 1) solution at −35 °C over a period of one month. The X-ray data for **2** and **3** were collected at 103(2) and 153(2) K, respectively, on a Bruker Apex CCD-based X-ray diffractometer equipped with a Mo X-ray tube (λ = 0.71073 Å). The frames were integrated with the Bruker SAINT Software package, and the data were corrected for absorption using the SADABS program. The structure was solved and refined using the Bruker SHELXTL software. All non-hydrogen atoms were refined anisotropically. Hydrogen atoms were placed at the calculated positions and were included in the final refinement using a riding model. Relevant crystallographic details are summarized in Table 6. The molecular geometries along with atomic labeling are represented in Fig. 2.

Table 6 Relevant crystallographic details and spherical atom refinement for **2** and **3**

	$Ph(CH_3)_2N$–O (**2**)	$Ph_2(CH_3)N$–O (**3**)
Formula	$C_8H_{11}NO$	$C_{13}H_{13}NO$
Fw	137.18	177.11
Cryst. syst.	Orthorhombic	Orthorhombic
Space group	*Pbca* (no. 61)	$Pna2_1$ (no. 33)
a/Å	6.8786(2)	23.660(3)
b/Å	10.6936(3)	15.685(2)
c/Å	20.2354(6)	5.5041(8)
V/Å^3	1488.46(7)	2042.6(5)
Z	8	8
ρ_{calc}/g cm^{-3}	1.224	1.296
μ/mm^{-1}	0.081	0.082
Radiation (λ, Å)	MoK_α (0.71073)	MoK_α (0.71073)
F(000)	592	848
Temp./K	103(2)	153(2)
Refinement method	Full matrix least square on F^2	
Data/rest/params	1311/0/135	2688/1/271
R_1, wR_2		
$I > 2\sigma(I)$	0.0288, 0.0759	0.0533, 0.0877
All data	0.0318, 0.0773	0.0912, 0.0969
GOF	1.077	0.894

High-angle X-ray experiments followed by multipole refinement

The multipole refinement for **2** was carried out within the Hansen–Coppens' formalism[42] with the XD program package.[43] The core and the spherical valence densities were composed of relativistic Dirac-Fock wave functions reported by Su, Coppens and Macchi (SCM data bank file).[44] Single-zeta functions with energy-optimized Slater exponents were used for the deformation density terms.[45] The refinement was carried out with respect to F^2 and converged to R = 0.0204 and GOF = 1.578 for 3254 merged reflections with $I > 3\sigma(I)$. All C–C and C–N bonded pairs of atoms satisfy the Hirschfeld rigid-bond criteria (the maximum difference of the mean-square displacement amplitudes was 9×10^{-4} Å^2). For the N–O bond, the corresponding value was slightly larger but did not exceed 12×10^{-4} Å^2. The residual electron density for reflections with $2\Theta < 90°$ was smaller than 0.185 e Å^{-3}. Topological analyses of the experimental $\rho(\mathbf{r})$ function were performed using the TOPXD[46] and WinXPRO[47] program packages (for more details see ESI†).

The kinetic energy density [$g(\mathbf{r})$] was estimated from the experimental diffraction data within the Kirzhnits's approximation,[48] which relates it to values of $\rho(\mathbf{r})$ and its derivatives (eqn (2)):

$$g(r) = \left(\frac{3}{10}\right)(3\pi^2)^{2/3}[\rho(r)]^{5/3} + \frac{\left(\frac{1}{72}\right)|\nabla\rho(r)|^2}{\rho(r)} + \left(\frac{1}{6}\right)\nabla^2\rho(r) \quad (2)$$

Use of this relationship in conjunction with the virial theorem (eqn (3))

$$[2g(r) + v(r)] = \tfrac{1}{4}\nabla^2\rho(r) \quad (3)$$

provided values of the potential energy density $v(\mathbf{r})$ at the critical point.

Computational

Geometry optimizations for all systems were carried out at the DFT level with the parameter-free hybrid exchange-correlation

Published on 10 January 2012 on http://pubs.rsc.org | doi:10.1039/C2CP22341D
Downloaded by Universite de Picardie on 27 November 2012

functional PBE0.[49] The augmented correlation-corrected triple-zeta basis sets (aug-cc-pVTZ) were applied for oxygen and nitrogen atoms while the carbon and hydrogen atoms were described with the cc-pVTZ basis sets. The use of single reference approaches accounting primarily for dynamic electron correlation is a reasonable choice for the computation of the geometry parameters. Symmetrical molecules such as $(CH_3)_3N$–O and Ph_3N–O were modeled under C_3 symmetry constraints. C_s symmetry constraints were applied for $Ph(CH_3)_2N$–O, **2**, while $Ph_2(CH_3)N$–O, **3**, was optimized without symmetry constraints (C_1 symmetry). Except for Ph_3N–O, the initial geometries were based on X-ray crystallographic structural data[50] with proper adjustments for the C–H bond lengths. For the optimized geometries, the norm of gradient was below 10^{-5} H $bohr^{-1}$. For all molecules, the presence of true minima was confirmed by the absence of imaginary frequencies in the calculated Hessian matrix and the subsequent determination of the harmonic frequencies. All geometry optimizations were performed with the TURBOMOLE (version 5.10) program package.[51]

Geometry optimizations at the MP2 level of the amines **1a–4a** and amine-*N*-oxides **1–4** were performed starting with the previously DFT(PBE0) optimized structures. All calculation were carried out with the parallelized ricc2 program of Turbomole (version 6.2) employing the resolution of identity (RI) method.[52] The augmented correlation-corrected quadruple-zeta basis sets (aug-cc-pVQZ) were applied for oxygen and nitrogen atoms while the carbon and hydrogen atoms were described with the cc-pVTZ basis sets. The corresponding auxiliary RI-basis sets were taken from the Turbomole (version 6.2) basis set library.[53]

The electronic structure of the molecules reported herein was analyzed in detail with the aid of the Natural Bond Orbitals (NBO) approach.[23] Bond orders quoted in the text are those from the Wiberg formula[54] (so-called Wiberg bond indexes) incorporated in the NBO analysis. The condensed on atoms Wiberg indexes were also analyzed. The donor–acceptor interactions were estimated by application of the second-order perturbation theory in the NBO basis. All computations were performed with help of GENNBO (version 5.0) program[55] using converged DFT/PBE0 wavefunctions generated by the Firefly/PCGAMESS[56] program package in single-point calculations with the same basis sets.

The DFT/PBE0 electron densities for all systems were analyzed in the framework of QTAIM.[9] The topological bond orders discussed in the text below were obtained as proposed by Tsirelson *et al.* shown in eqn (4),[14]

$$n_{\mathrm{topo}} = a_0 + a_1(\lambda_1 + \lambda_2) + a_3\lambda_3 + a_3\rho_{\mathrm{BCP}} \qquad (4)$$

where ρ_{BCP} corresponds to the value of the electron density at the bond critical point and λ_1, λ_2, λ_3 are the eigenvalues of the Hessian of the electron density at the BCP. The values of the three parameters (a_1, a_2, a_3) were taken from the original paper.[14] These parameters were statistically derived based on a large set of calculated and experimentally available electron densities of molecules, which contain different types of N–O bonds (63 samples). Topological analyses were carried out using the AIM2000 and AIMALL program suites.[57] The program DGrid[58] (version 4.3) was used for the visualization of 3D plots of the Laplacian function, of the one electron potential (OEP) and the electron localization function (ELF).

The DFT optimized geometries were used in the next step for high-level multireference calculations using CASSCF and subsequent MCQDPT2 techniques.[59] No geometry optimization was carried out at these levels. At the first stage, the conventional CASSCF computation was performed with the active space comprised by three doubly occupied molecular orbitals (MO) corresponding to the σ-N–O bond and two *p*-shaped lone pairs centered on the oxygen atom as well as three unoccupied MOs. Thus, six electrons were correlated with 6 orbitals (CASSCF(6,6) approach). The MCQDPT2 calculations were carried out with the reference wavefunctions of the preceding CASSCF calculations. The conventional intruder state avoidance technique[60] was used with a shift value of 0.02 a.u. in the MCQDPT2 calculations. To achieve better convergence, no symmetry constraints were applied during these high-level single-point calculations. All multireference calculations were performed using the Firefly/PCGAMESS program package (ver. 7.1.9.F.),[56] which is partially based on the GAMESS-US source code.[61]

The periodic boundary calculation for trimethylamine-*N*-oxide, **1**, was calculated with the Crystal09 program package[62] using the published crystal structure data of **1**[12] in *C*2/*m* space group (no. 12) as starting point for the optimization. Both the lattice and geometrical parameters were optimized employing the 6-21G* (carbon and nitrogen atoms) and 6-31G* (oxygen and hydrogen atoms) basis sets.

The geometry of trimethylamine-*N*-oxide, **1**, was also optimized with the parallel version of the CFOUR program package (ver. 1.0)[63] at the CCSD(T) level using aug-cc-pVQZ basis sets for the nitrogen and oxygen atoms and cc-pVTZ basis sets for the residual atoms.

Acknowledgements

Funding by Deutsche Forschungsgemeinschaft (Priority Programme SPP 1178) is gratefully acknowledged.

References

1 W. R. Wilson, W. A. Denny, S. M. Pullen, K. M. Thompson, A. E. Li, L. H. Patterson and H. H. Lee, *Br. J. Cancer*, 1996, **74**, S43.
2 *Recent and selected papers*: (*a*) S. Jamal, N. K. Poddar, L. R. Singh, T. A. Dar, V. Rishi and F. Ahmad, *FEBS J.*, 2009, **276**, 6024; (*b*) D. L. Pincus, C. Hyeon and D. Thirumalai, *J. Am. Chem. Soc.*, 2008, **130**, 7364; (*c*) V. Doan-Nguyen and J. P. Loria, *Protein Sci.*, 2007, **16**, 20; (*d*) P. Attri, P. Venkatesu and M.-J. Lee, *J. Phys. Chem. B*, 2010, **114**, 1471; (*e*) B. Gong, L. Y. Zhang, C.-P. Pang, D. S.-C. Lam and G. F.-H. Yam, *Mol. Vision*, 2009, **15**, 2829; (*f*) P. H. Yancey, M. E. Clark, S. C. Hand, R. D. Bowlus and G. N. Somero, *Science*, 1982, **217**, 1214.
3 *Recent articles and reviews*: (*a*) B. J. Bennion and V. Daggett, *Proc. Natl. Acad. Sci. U. S. A.*, 2004, **101**, 6433; (*b*) S. Paul and G. N. Patey, *J. Am. Chem. Soc.*, 2007, **129**, 4476; (*c*) L. M. F. Holthauzen, J. Rösgen and D. W. Bolen, *Biochemistry*, 2010, **49**, 1310; (*d*) Y. X. Qu, C. L. Bolen and D. W. Bolen, *Proc. Natl. Acad. Sci. U. S. A.*, 1998, **95**, 4831; (*e*) A. Panuszko, P. Bruździak, J. Zielkiewicz, D. Wyrzykowsky and J. Stangret, *J. Phys. Chem. B*, 2009, **113**, 14797; (*f*) F. Meersman, D. Bowron, A. K. Soper and M. H. J. Koch, *Biophys. J.*, 2009, **97**, 2559.
4 (*a*) A. D. Di Michele, M. Freda, G. Onori and A. Santucci, *J. Phys. Chem. A*, 2004, **108**, 6145; (*b*) Q. Zou, B. J. Bennion, V. Daggett and K. P. Murphy, *J. Am. Chem. Soc.*, 2002, **124**, 1192.
5 *Recent papers and reviews*: (*a*) H. Wei, Y. Fan and Y. Q. Gao, *J. Phys. Chem. B*, 2010, **114**, 557; (*b*) C. Y. Hu, G. C. Lynch,

 This journal is © the Owner Societies 2012

View Article Online

Published on 10 January 2012 on http://pubs.rsc.org | doi:10.1039/C2CP22341D
Downloaded by Universite de Picardie on 27 November 2012

H. Kokubo and B. M. Pettitt, *Proteins*, 2010, **78**, 695; (*c*) M. V. Athawale, J. S. Dordick and S. Garde, *Biophys. J.*, 2005, **89**, 858; (*d*) B. J. Bennion, M. L. DeMarco and V. Daggett, *Biochemistry*, 2004, **43**, 12955; (*e*) S. Paul, *Chem. Phys.*, 2010, **368**, 7; (*f*) G. Stirnemann, J. T. Hynes and D. Laage, *J. Phys. Chem. B*, 2010, **114**, 3052; (*g*) N. Biyani and S. Paul, *J. Phys. Chem. B*, 2009, **113**, 9644; (*h*) M. V. Athawale, S. Sarupria and S. Garde, *J. Phys. Chem. B*, 2008, **112**, 5661; (*i*) J. Qvist and B. Halle, *J. Am. Chem. Soc.*, 2008, **130**, 10345; (*j*) A. Fornili, M. Civera, M. Sironi and S. L. Fornili, *Phys. Chem. Chem. Phys.*, 2003, **5**, 4905; (*k*) S. Paul and G. N. Patey, *J. Phys. Chem. B*, 2006, **110**, 10514; (*l*) M. Freda, G. Onori and A. Santucci, *J. Phys. Chem. B*, 2001, **105**, 12714; (*m*) K. M. Kast, J. Brickmann, S. M. Kast and R. S. Berry, *J. Phys. Chem. A*, 2003, **107**, 5342; (*n*) D. A. C. Beck, B. J. Bennion, D. O. V. Alonso and V. Daggett, in *Methods in Enzymology*, ed. D. Häussinger and H. Sies, Elsevier, 2007, vol. 428 (ch. 22).

6 (*a*) G. Rousselet, C. Chassagnard, P. Capdevielle and M. Maumy, *Tetrahedron Lett.*, 1996, **37**, 8497; (*b*) K. B. Sharpless, K. Akashi and K. Oshima, *Tetrahedron Lett.*, 1976, **29**, 2503; (*c*) K. S. Shin and H. M. Goff, *J. Am. Chem. Soc.*, 1987, **109**, 3140; (*d*) T. Y. Luh, *Coord. Chem. Rev.*, 1984, **60**, 225; (*e*) M. O. Albers and N. J. Coville, *Coord. Chem. Rev.*, 1984, **53**, 227; (*f*) J.-K. Shen, Y.-C. Gao, Q.-Z. Shi and F. Basolo, *Organometallics*, 1989, **8**, 2144; (*g*) Y.-L. Shi, Y.-C. Gao, D. L. Kershner and F. Basolo, *Organometallics*, 1987, **6**, 1528; (*h*) J.-K. Shen, Y.-C. Gao, Q.-Z. Shi and F. Basolo, *Inorg. Chem.*, 1988, **27**, 4236; (*i*) Y.-C. Gao, Q.-Z. Shi, D. L. Kershner and F. Basolo, *Inorg. Chem.*, 1988, **27**, 188.

7 (*a*) S. D. Nelson, P. A. Kollman, W. F. Trager and S. Rothenberg, *J. Med. Chem.*, 1973, **16**, 1034; (*b*) F. Choplin and G. Kaufmann, *J. Mol. Struct.*, 1972, **11**, 381; (*c*) A. Haaland, H. Thomassen and Y. Stenstrøm, *J. Mol. Struct.*, 1991, **263**, 299; (*d*) K. Kast, S. Reiling and J. Brickmann, *J. Mol. Struct.: THEOCHEM*, 1998, **453**, 169; (*e*) R. Noto, V. Martorana, A. Emanuele and S. A. Fornili, *J. Chem. Soc., Faraday Trans.*, 1995, 3803.

8 (*a*) T. Zheng-Xin, L. Xiao-Hong and Z. Xian-Zhou, *J. Mol. Struct.: THEOCHEM*, 2009, **907**, 126; (*b*) T. Zheng-Xin, L. Xiao-Hong, Z. Rui-Zhou and Z. Xian-Zhou, *J. Theor. Comput. Chem.*, 2009, **8**, 541; (*c*) K. V. Berezin, *Opt. Spectra*, 2003, **94**, 209; (*d*) R. B. Perni, P. J. Kowalczyk, A. M. Treasurywala and M. Tracy, *Tetrahedron Lett.*, 1995, **36**, 699; (*e*) O. Mó, M. Yáñez, A. L. Llamas-Saiz, C. Foces-Foces and J. Elguero, *Tetrahedron*, 1995, **51**, 7045; (*f*) M. Boiani, H. Cerecetto, M. Gonzáles, O. E. Piro and E. E. Castellano, *J. Phys. Chem. A*, 2004, **108**, 11241; (*g*) J. Berdys, M. Makowski, M. Makowska, A. Puszko and L. Chmurzyński, *J. Phys. Chem. A*, 2003, **107**, 6293; (*h*) M. Yamakawa, K. Ezumi, Y. Mizuno and T. Kubota, *Bull. Chem. Soc. Jpn.*, 1974, **47**, 2982; (*i*) N. Mariet, M. Ibrahin-Ouali, J.-L. Parrain and M. Santelli, *J. Mol. Struct.: THEOCHEM*, 2004, **679**, 53; (*j*) G. V. Kulkarni, A. Ray and C. C. Patel, *J. Mol. Struct.*, 1981, **71**, 253; (*k*) A. Hinchliffe, *J. Mol. Struct.*, 1977, **41**, 159; (*l*) K. Szczepaniak, W. B. Person and D. Hadži, *J. Phys. Chem. A*, 2005, **109**, 6710; (*m*) J. Panek, J. Stare and D. Hadži, *J. Phys. Chem. A*, 2004, **108**, 7417; (*n*) Y. Kobayashi, I. Kunadaki and H. Sato, *Tetrahedron Lett.*, 1970, **27**, 2337; (*o*) C. Leibovici and J. Streith, *Tetrahedron Lett.*, 1971, **5**, 387.

9 (*a*) R. F. W. Bader, *Atoms in Molecules: A Quantum Theory*, Clarendon Press, Oxford, 1990; (*b*) *The Quantum Theory of Atoms in Molecules*, ed. C. F. Matta and R. J. Boyd, Wiley-VCH Verlag, 2007.

10 J.-K. Shen, Y.-C. Gao, Q.-Z. Shi and F. Basolo, *J. Organomet. Chem.*, 1991, **401**, 295.

11 The POAV is the p-orbital axis vector introduced by Haddon *et al.* in: R. C. Haddon, *J. Am. Chem. Soc.*, 1990, **112**, 3385. This angle theta (or 90-theta) is also a good measure for the deviation from planarity. It is 90° for planar systems, 101.04° for the ball-shaped buckminsterfullerene and 109.5° for a tetrahedral carbon atom.

12 A. Caron, G. J. Palenik, E. Goldfish and J. Donohue, *Acta Crystallogr.*, 1964, **17**, 102.

13 F. Choplin and G. Kaufmann, *Spectrochim. Acta, Part A*, 1970, **26**, 2113.

14 V. G. Tsirelson, E. V. Bartashevich, A. I. Stash and V. A. Potemkin, *Acta Crystallogr., Sect. B: Struct. Sci.*, 2007, **63**, 142.

15 A positive value of $\nabla^2\rho(\mathbf{r})$ is not a unique criterion for a closed-shell interaction, however. The necessary condition for this type of interaction is a positive value of the energy density, which is related to $\nabla^2\rho(\mathbf{r})$ by equation $h_e(\mathbf{r}) = v(\mathbf{r}) + g(\mathbf{r}) = g(\mathbf{r}) - \nabla^2\rho(\mathbf{r})$, where $v(\mathbf{r})$ and $g(\mathbf{r})$ are the potential and kinetic energy densities, respectively. The value of $h_e(\mathbf{r})$ may still remain negative if the potential energy density (*a priori* negative) exceeds the kinetic energy density in absolute value. Therefore, the bonds which are characterized by a positive value of $\nabla^2\rho(\mathbf{r})$ and a negative value of $h_e(\mathbf{r})$ are referred to as an intermediate type of interatomic interaction. The opposite situation is commonly observed for the shared type of interaction. In that case, one can interpret it as the contribution of an ionic interaction (closed-shell type) to the mainly covalent one. The latter can be considered as a polar covalent bond.

16 (*a*) J. A. Dobado, H. Martínes-Garćia, J. Molina and M. R. Sundberg, *Prog. Theor. Chem. Phys.*, 2000, **3**, 337 Quantum Systems in Chemistry and Physics, Vol. 2; (*b*) I. Alkorta and J. Elguero, *J. Phys. Chem. A*, 1999, **103**, 272; (*c*) J. A. Dobado, H. Martínes-Garćia, J. Molina and M. R. Sundberg, *J. Am. Chem. Soc.*, 1998, **120**, 8461.

17 *Selected reviews*: (*a*) U. Koch and P. L. Popelier, *J. Phys. Chem.*, 1995, **99**, 9747; (*b*) G. R. Desiraju, *Acc. Chem. Res.*, 1996, **29**, 441; (*c*) E. Espinosa, M. Souhasson, H. Lachekar and C. Lecomte, *Acta Crystallogr., Sect. B: Struct. Sci.*, 1999, **55**, 563; (*d*) *Theoretical Treatment of Hydrogen Bonding*, ed. D. Hadži, Wiley-VCH Verlag, 1997; (*e*) G. R. Desiraju, *Acc. Chem. Res.*, 2002, **35**, 565; (*f*) G. R. Desiraju, *Chem. Commun.*, 2005, 2995; (*g*) R. K. Castellano, *Curr. Org. Chem.*, 2004, **8**, 845; (*h*) K. Biradha, *CrystEngComm*, 2003, **5**, 374.

18 T. Steiner and W. Saenger, *J. Am. Chem. Soc.*, 1992, **114**, 10146.

19 (*a*) G. A. Jeffrey and W. Saenger, *Hydrogen Bonding in Biological Structures*, Springer, Berlin, 1991; (*b*) W. Saenger, *Principles of Nucleic Acid Structure*, Springer, Berlin, 1984.

20 T. Steiner and W. Saenger, *J. Am. Chem. Soc.*, 1993, **115**, 4540.

21 (*a*) E. Espinosa, E. Molins and C. Lecomte, *Chem. Phys. Lett.*, 1998, **285**, 170; (*b*) E. Espinosa, I. Alkorta, I. Rozas, J. Elguero and E. Molins, *Chem. Phys. Lett.*, 2001, **336**, 457.

22 (*a*) K. A. Lyssenko, Yu. V. Nelyubina, R. G. Kostyanovsky and M. Yu. Antipin, *ChemPhysChem*, 2006, **7**, 2453; (*b*) K. A. Lyssenko, A. A. Korlyukov and M. Yu. Antipin, *Mendeleev Commun.*, 2005, 90; (*c*) I. V. Glukhov, K. A. Lyssenko, A. A. Korlyukov and M. Yu. Antipin, *Faraday Discuss.*, 2007, **135**, 203; (*d*) K. A. Lyssenko and M. Yu. Antipin, *Russ. Chem. Bull.*, 2006, **55**, 1; (*e*) K. A. Lyssenko, A. A. Korlyukov, D. G. Golovanov, S. Yu. Ketkov and M. Yu. Antipin, *J. Phys. Chem. A*, 2006, **110**, 6545.

23 (*a*) F. Weinhold and C. A. Landis, *Valency and Bonding: A Natural Bond Orbital Donor–Acceptor Perspective*, Cambridge University Press, Cambridge, 2005; (*b*) A. E. Reed, L. A. Curtiss and F. Weinhold, *Chem. Rev.*, 1988, **88**, 899.

24 (*a*) M. D. Burtzoff, L. Peter, P. A. Lepse and D. Y. Zhang, *J. Mol. Struct.: THEOCHEM*, 2002, **619**, 229; (*b*) A. E. Reed and P. R. Schleyer, *J. Am. Chem. Soc.*, 1990, **112**, 1434.

25 In terms of natural orbitals obtained as from the multireference calculations, *e.g.* CASSCF, the bond order, BO, for the selected bond can be calculated from the set of bonding and anti-bonding NOs according to

$$\mathrm{BO} = \frac{\sum_i n_i(\text{bonding}) - \sum_j n_j(\text{anti-bonding})}{2},$$

where $n_{i,j}$ is the population of the corresponding orbital.

26 (*a*) M. Lein and G. Frenking, *Theory and Applications of Computational Chemistry*, ed. C. Dykstra, 2005, ch. 13; (*b*) M. Lein, A. Szabó, A. Kovács and G. Frenking, *Faraday Discuss.*, 2003, **124**, 365; (*c*) G. Frenking, K. Wichmann, N. Fröhlich, C. Loschen, M. Lein, J. Frunzke and V. M. Rayón, *Coord. Chem. Rev.*, 2003, **238–239**, 55; (*d*) M. P. Mitoraj, A. Michalak and T. Ziegler, *J. Chem. Theory Comput.*, 2009, **5**, 962; (*e*) M. Mitoraj, H. Zhu, A. Michalak and T. Ziegler, *J. Org. Chem.*, 2006, **71**, 9208; (*f*) T. Ziegler and A. Rauk, *Theor. Chim. Acta*, 1977, **46**, 1.

27 A. N. Sobolev, V. K. Belsky, I. P. Romm, N. Yu. Chernikova and E. N. Guryanova, *Acta Crystallogr., Sect. C: Cryst. Struct. Commun.*, 1985, **41**, 967.

28 S. Ikuta and P. Kebarle, *Can. J. Chem.*, 1983, **61**, 97.

29 A. J. Blake, A. V. Ebswoth and A. J. Welch, *Acta Crystallogr., Sect. C: Cryst. Struct. Commun.*, 1984, **40**, 413.

30 (*a*) V. A. Naumov, S. Samdal, A. V. Naumov, S. Gundersen and H. V. Volden, *Russ. J. Gen. Chem.*, 2005, **75**, 1956; (*b*) Y. Sasaki, K. Kimura and M. Kubo, *J. Chem. Phys.*, 1959, **31**, 477.

View Article Online

Downloaded by Universite de Picardie on 27 November 2012
Published on 10 January 2012 on http://pubs.rsc.org | doi:10.1039/C2CP22341D

31 (*a*) H. B. Lueck, J. L. McHale and W. D. Edwards, *J. Am. Chem. Soc*., 1992, **114**, 2342; (*b*) G. Meijer, G. Berden, W. L. Meerts, H. E. Hunziker, M. S. de Vries and H. R. Wendt, *Chem. Phys*., 1992, **163**, 209; (*c*) A. N. Rodionov, N. I. Ruch'eva, K. L. Rogozin and D. N. Shigorin, *Zh. Prikl. Sprectrosk*., 1974, **20**, 534; (*d*) P. Knobloch and M. Stockhausen, *Angew. Chem., Int. Ed. Engl*., 1964, **3**, 230; (*e*) R. D. W. Kemmitt, R. H. Nuttall and D. W. A. Sharp, *J. Chem. Soc*., 1960, 46; (*f*) I. Reva, L. Lapinsky, N. Chattopadhyay and R. Fausto, *Phys. Chem. Chem. Phys*., 2003, **5**, 3844.

32 (*a*) C. B. Duke, R. W.-O. Lin, A. Paton, W. R. Salaneck and K. L. Yip, *Chem. Phys. Lett*., 1979, **61**, 402; (*b*) M. Malagoli and J. L. Brédas, *Chem. Phys. Lett*., 2000, **327**, 13; (*c*) J. Pacansky, R. J. Waltman and H. Seki, *Bull. Chem. Soc. Jpn*., 1997, **70**, 55.

33 M. Tanaka and M. Aida, *Chem. Phys. Lett*., 2006, **417**, 316.

34 V. I. Stenberg and J. E. Schiller, *J. Am. Chem. Soc*., 1975, **97**, 424.

35 (*a*) E. N. Lassettre, *J. Chem. Phys*., 1985, **83**, 1709; (*b*) G. Hunter, *Int. J. Quantum Chem*., 1986, **29**, 197.

36 (*a*) A. D. Becke and K. E. Edgecombe, *J. Chem. Phys*., 1990, **92**, 5397; (*b*) A. Savin, O. Jepsen, J. Flad, O. K. Andersen, H. Preuss and H. G. von Schnering, *Angew. Chem., Int. Ed. Engl*., 1991, **31**, 187.

37 R. J. Gillspie and P. L. Popelier, *Chemical Bonding and Molecular Geometry*, Oxford University Press, New York, 2001.

38 R. Boese, D. Bläser, M. Yu. Antipin, V. Chaplinski and A. de Meijere, *Chem. Commun*., 1998, 781.

39 (*a*) J. Beckmann and S. Grabowsky, *J. Phys. Chem. A*, 2007, **111**, 2011; (*b*) A. M. Belostotskii, H. E. Gottlieb and M. Shokhen, *J. Org. Chem*., 2002, **67**, 9257; (*c*) A. K. Chandra, S. Parveen, S. Das and T. Zeegers-Huyskens, *J. Comput. Chem*., 2008, **29**, 1490; (*d*) J. W. M. Carniero, J. F. Dias, J. C. R. Tostes, P. R. Seidl and C. A. Taft, *Int. J. Quantum Chem*., 2003, **95**, 322; (*e*) Y. V. Vishnevskiy, M. A. Abaev, A. A. Ivanov, L. V. Vilkov and M. Dakkouri, *J. Mol. Struct*., 2008, **889**, 316; (*f*) V. Barone, J. E. Peralta, R. H. Contreras, A. V. Sosnin and V. D. Krivdin, *Magn. Reson. Chem*., 2001, **39**, 600.

40 E. V. Anslyn and D. A. Dougherty, *Modern Physical Organic Chemistry*, University Science Books, Mill Valley, USA, 2006.

41 J. C. Craig and K. K. Purushothaman, *J. Org. Chem*., 1970, **35**, 1721.

42 N. K. Hansen and P. Coppens, *Acta Crystallogr., Sect. A: Cryst. Phys., Diffr., Theor. Gen. Crystallogr*., 1978, **34**, 909.

43 A. Volkov, P. Macchi, L. J. Farrugia, C. Gatti, P. R. Mallinson and T. Koritsanszky, *XD2006, A Computer Program Package for Multipole Refinement, Topological Analysis of Charge Densities and Evaluation of Intermolecular Energies from Experimental or Theoretical Structure Factors*, 2006.

44 (*a*) Z. Su and P. Coppens, *Acta Crystallogr., Sect. A: Found. Crystallogr*., 1998, **54**, 646; (*b*) P. Macchi and P. Coppens, *Acta Crystallogr., Sect. A: Found. Crystallogr*., 2001, **14**, 656.

45 A similar procedure was used in the following investigations: (*a*) H. Ott, C. Däschlein, D. Leusser, D. Schildbach, T. Seibel, D. Stalke and C. Strohmann, *J. Am. Chem. Soc*., 2008, **190**, 11901; (*b*) S. Deuerlein, D. Leusser, U. Flierler, H. Ott and D. Stalke, *Organometallics*, 2008, **27**, 2306.

46 A. Volkov, C. Gatti, Yu. Abramov and P. Coppens, *Acta Crystallogr., Sect. A: Found. Crystallogr*., 2002, **56**, 252.

47 A. Stash and V. Tsirelson, *J. Appl. Crystallogr*., 2002, **35**, 371.

48 D. A. Kirzhnits, *J. Exp. Theor. Phys*., 1957, **5**, 54.

49 (*a*) J. P. Perdew, K. Burke and M. Enzerhof, *Phys. Rev. Lett*., 1997, **78**, 1396; (*b*) J. P. Perdew, K. Burke and M. Enzerhof, *Phys. Rev. Lett*., 1996, **77**, 3865.

50 For $(CH_3)_2PhN$–O and $(CH_3)Ph_2N$–O structural data were obtained within this study. The geometrical parameters for $(CH_3)_3N$–O, **1**, were taken from ref. 12.

51 R. Ahlrichs, M. Bär, M. Häser, H. Horn and C. Kölmel, *Chem. Phys. Lett*., 1989, **162**, 165.

52 C. Hättig, A. Hellweg and A. Köhn, *Phys. Chem. Chem. Phys*., 2006, **8**, 1159. TURBOMOLE V6.2 2010, a development of University of Karlsruhe and Forschungszentrum Karlsruhe GmbH, 1989–2007, TURBOMOLE GmbH, since 2007; available from http://www.turbomole.com.

53 F. Weigend, A. Köhn and C. Hättig, *J. Chem. Phys*., 2001, **116**, 3175.

54 K. Wiberg, *Tetrahedron*, 1968, **24**, 1083.

55 E. D. Glendening, J. K. Badenhoop, A. E. Reed, J. E. Carpenter, J. A. Bohmann, C. M. Morales and F. Weinhold, *NBO 5.0*., Theoretical Chemistry Institute, University of Wisconsin, Madison, 2001.

56 A. A. Granovsky, PC GAMESS/Firefly version 7.1.9, http://classic.chem.msu.su/gran/gamess/index.html.

57 (*a*) F. Biegler-König, J. Schönbohm and D. Bayles, *J. Comput. Chem*., 2001, **22**, 545; (*b*) T. A. Keith, *AIMAll (Version 10.11.24)*, 2010 (aim.tkgristmill.com).

58 M. Kohout, *Dgrid 4.3*, 2008.

59 H. A. Witek, Y.-K. Choe, J. P. Finley and K. Hirao, *J. Comput. Chem*., 2002, **23**, 957.

60 H. Nakano, *J. Chem. Phys*., 1993, **99**, 7983.

61 M. W. Schmidt, K. K. Baldridge, J. A. Boatz, S. T. Elbert, M. S. Gordon, J. H. Jensen, S. Koseki, N. Matsunaga, K. A. Nguyen, S. Su, T. L. Windus, M. Dupuis and J. A. Montgomery, *J. Comput. Chem*., 1993, **14**, 1347.

62 R. Dovesi, R. Orlando, B. Civalleri, C. Roetti, V. R. Saunders and C. M. Zicovich-Wilson, *Z. Kristallogr*., 2005, **220**, 571; R. Dovesi, V. R. Saunders, C. Roetti, R. Orlando, C. M. Zicovich-Wilson, F. Pascale, B. Civalleri, K. Doll, N. M. Harrison, I. J. Bush, P. D'Arco and M. Llunell, *CRYSTAL09, 2009 CRYSTAL09 User's Manual*, University of Torino, Torino, 2000.

63 M. E. Harding, T. Metzroth, J. Gauss and A. A. Auer, *J. Chem. Theory Comput*., 2008, **4**, 64.

 This journal is © the Owner Societies 2012